Converging gravity currents of power-law fluid

Published:
DOI: http://doi.org/10.1017/jfm.2021.305

Longo, S., Chiapponi, L., Petrolo, D., Lenci, A., & Di Federico, V. (2021). Converging gravity currents of power-law fluid. ***Journal of Fluid Mechanics, 918*****.**

https://doi.org/10.1017/jfm.2021.305

accepted on March 2021

Converging gravity currents of power-law fluid

S. Longo[1], L. Chiapponi[1], D. Petrolo[1], A. Lenci[2], V. Di Federico[2]

[1]Department of Engineering and Architecture - Università degli Studi di Parma - Parco Area delle Scienze 181/A - 43124 Parma - Italy

[2]Department of Civil, Chemical, Environmental, and Materials Engineering - Alma Mater Studiorum Università di Bologna - Viale Risorgimento 2 - 40136 Bologna - Italy

(Received)

We study non-Newtonian effects associated with power-law rheology of behaviour index n on the propagation of horizontal gravity currents. Two different setups are examined: i) converging flow toward the origin in a channel of gap thickness $b(x) \propto x^k$ and $k < 1$ and ii) converging flow along r toward the centre in a cylinder. The front of the current propagates in the negative x or r direction reaching the origin in a finite touch-down time t_c during the pre-closure phase; in the post-closure phase, the current flows back in the positive direction and progressively levels out. Under the classical viscous-buoyancy balance, the current propagation is described by a differential problem amenable to a self-similar solution of the second-kind coupling space and reduced time $t_r = t_c - t$. The problem formulation in the phase plane brings to an autonomous system of differential equations which requires numerical integration and yields the shape of the current and its front as $\xi_f \propto t_r^{\delta_c}$, ξ_f being the self-similar variable value at the front and δ_c being the critical eigenvalue. The latter is a function of fluid rheology n and of channel geometry k for the first setup; it is a function only of n for the second setup. The dependency on n is modest. The theoretical formulation is validated through experiments conducted during both pre- and post-closure phases and aimed at measuring the front position and the profile of the current. Experimental results are in fairly good agreement with theory and allow quantitative determination of the time interval of validity of the intermediate asymptotics regime, when self-similarity is achieved and when is lost.

Key words: gravity currents, second-kind self-similarity, intermediate asymptotics, non-Newtonian, Hele-Shaw cell

1. Introduction

Gravity driven flows under a viscous regime are recurrent in the industry (outflow from plants, process engineering applications) and environment (both in surface and subsurface domains) (Simpson 1982; Huppert 2006). These phenomena are described by nonlinear diffusion equations with counterparts in several fields of physics, such as heat conduction by electrons and by radiation, or flow in porous media under the Dupuit-Forchheimer approximation (Diez *et al.* 1992*a*). In many applications having a simple geometry, the spreading is adequately described by self-similar solutions of the first-kind, representing intermediate asymptotics according to the definition by Barenblatt (Barenblatt & Zel'Dovich 1972). In this case the variables that entangle space and time (these are the two independent variables in most problems) can be found on the basis of concepts of simple dimensional analysis. The seminal publications by Huppert (1982) and Didden & Maxworthy (1982), later extended to porous media flow in plane (Huppert & Woods 1995) and axisymmetric geometry (Lyle *et al.* 2005), are relevant examples of the application of first-kind self-similarity to modelling the free-surface advancement of Newtonian fluids into air or another fluid.

Extensions of this kind of modelling to non-Newtonian rheology, mainly of power-law nature, were first due to Aronsson & Janfalk (1992), Kondic *et al.* (1996) and Kondic *et al.* (1998): these works deal with the analysis of fingering in Hele-Shaw cells. A contribution devoted to bubble contraction analysis in a Hele-Shaw cell for the case in which the surrounding fluid is of power-law type is due to McCue & King (2011). Further contributions of interest are Gratton *et al.* (1999); Perazzo & Gratton (2003); Di Federico *et al.* (2012) and Perazzo & Gratton (2005); Longo *et al.* (2015*b*). The combined effect of rheology and confining boundaries was analysed in Longo *et al.* (2015*a*).

More variegate are the theoretical and experimental studies of gravity currents in fractures (Di Federico 1998) and in porous media, possibly with variable permeability and analysing the coupled effect of non-Newtonian rheology and spatial heterogeneity; (see Lauriola *et al.* 2018, and references therein).

Pressurized flows of power-law fluids in porous media with variable conductivity are also amenable to self-similar solutions of the first-kind (Ciriello *et al.* 2013); the same holds for unsteady flows of shear-thinning fluids in infinite domains with pressure-dependent properties and different geometries, due to a generalized formulation incorporating the three main cases: plane, radial and spherical (Longo & Di Federico 2015).

A key step in the process of looking for a self-similar solution to a propagation problem is the individuation of the transformation (a group) that combines two independent variables, space and time, into a single one, thus reducing a set of partial differential equations (PDE) into an ordinary differential equation (ODE), provided the initial and boundary conditions coalesce as well. The fundamental element is the principle of general covariance in physics: whenever we individuate a transformation that leaves a mathematical problem invariant, the best and in minimum number variables completely describing that problem are invariant within the same transformation. A power function structure of the terms involved in the differential problem is propitious for self-similar solutions, and this justifies the choice, as a trial set-up, of a variation of the channel gap $\propto x^k$. Managing an ODE is by far simpler than solving a PDE, and allows in some cases analytical solutions. The transformation is mostly of the form $\xi = x/t^\beta$ (a well known exception is the transformation $\xi = ct - x$, c being celerity, adopted in solving wave propagation problems on the surface of heavy fluids, see Stokes (1880), although this case too can be reduced to the standard power form, see Gratton & Minotti (1990)) where the exponent β is obtained by balancing the dimensions of all terms of the equations, including initial and boundary conditions. The solution to the resulting ordinary (nonlinear) differential problem represents the system behaviour in an intermediate time interval: not too early, as initial and boundary conditions at an early stage still control the details of the flow; not too late since, in general, the solutions do not describe properly the ultimate equilibrium state of the system (Barenblatt 1996), mainly due to the instability of the solution under small perturbations or to inconsistencies in balances when time tends to infinity.

Another class of propagation problems is again self-similar, as shown by numerical integration or by experiments, but the evaluation of the exponent β is impossible simply via dimensional analysis; the solution of the whole problem is required, with a procedure similar to the determination of eigenvalues in linear problems. This type of self-similarity is quoted as “second-kind” or “incomplete similarity”; an indicator of a possible self-similarity of second-kind is the presence of scales of the problem in excess, with fewer dimensional equations than variables (Barenblatt 2003).

Early analyses of these kind of solutions for gravity currents are due to Gratton & Minotti (1990); Diez *et al.* (1992*a*,*b*); Aronson & Graveleau (1993); Angenent & Aronson (1995*a*,*b*); Aronson *et al.* (2003). The work by Zheng *et al.* (2014) accounts for second-kind self-similar solutions arising in converging flows in heterogeneous porous media. A subsequent contribution adopted a similar setup and developed a theoretical and experimental analysis in the presence of a permeable substrate (Zheng *et al.* 2015).

A general approach containing the tools for selecting first-kind and second-kind self-similar solution is the phase-plane formalism, described in the context of viscous gravity currents by Gratton & Minotti (1990), and applied also to inviscid gravity currents by Slim & Huppert (2004). A general description of singularities and their role in second-kind self-similar solution, in the context of phase-plane formalism, is contained in Eggers & Fontelos (2015). The phase-plane formalism is adopted also in Daly & Porporato (2004), where different classes of problems connected to mathematical hydraulics and non-Newtonian fluids are discussed. In many cases, numerical methods are used for integration, although an asymptotic approach has also been developed, based on the idea that some second-kind similarity solutions can be viewed as a perturbation of problems with known similarity solution (Cole & Wagner 1996; Wagner 2005).

The present work focuses on the theoretical and experimental analysis of gravity currents of power-law fluids in a context where a second kind of self-similarity is expected. The power-law rheology is the simplest model that approximates the behaviour of a non-Newtonian fluid in which the strain rate is scaled non-linearly with applied stress, a category of fluids that is widespread not only in environmental flows on the surface (Coussot & Meunier 1996) but also in the food industry (Lareo *et al.* 1997), sewage treatment (Eshtiaghi *et al.* 2013), biomechanics (Carpenter *et al.* 2020), oil and gas drilling systems (Epelle & Gerogiorgis 2020) and pipeline flow (Livescu 2012). Its limitation is being valid over only a limited range of shear rates, hence its properties depend on the range of shear rates taken into account. Yet, it constitutes the most frequently adopted model in engineering applications.

The possibility to have reliable solutions to adopt as benchmarks for the asymptotic behaviour of numerical solutions, and to extract relevant scalings for the front speed and depth of gravity currents, justifies the extension of the analyses already available in literature for a Newtonian fluid to the power-law model. The two specific settings examined both involve converging gravity currents and are: i) a horizontal channel or fracture of variable width, and ii) an axisymmetric geometry. Analytical solutions and numerical results based on second-kind self-similarity adopting the phase-plane formalism are derived for both the pre-closure phase (before the current nose reaches the origin) and the post-closure phase (after the nose reaches the origin and the current flows back). The first theoretical results in axisymmetric geometry are due to Gratton & Perazzo (2010), results confirmed in the present work and extended to experimental verification.

The manuscript is structured as follows. Section 2 presents the problem formulation for the horizontal channel and its solution, while Section 3 contains the same analysis for radial geometry. Section 4 provides details on the experimental setups and on three sets of experiments, comparing the theoretical and experimental positions of the front of the current and its profiles for both pre- and post-closure phase. Section 5 contains the conclusion. Two Appendices complete the paper. Appendix A reports the numerical values of the critical eigenvalue δ_c governing self-similar propagation for the two setups; Appendix B describes plane flow of a power-law fluid converging toward the origin in a

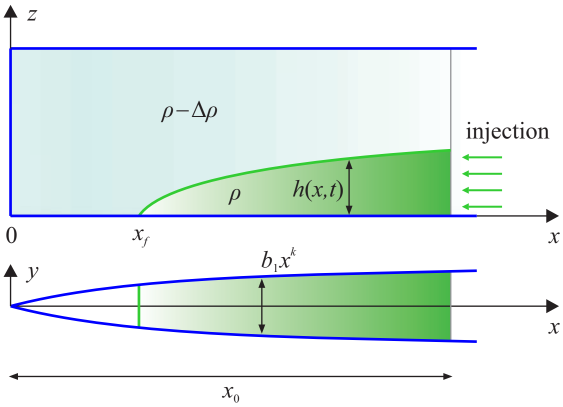

FIGURE 1. Horizontal channel with varying gap thickness b_1x^k: a converging gravity current in viscous-buoyancy balance propagates toward the origin. x_f is the instantaneous front position, x_0 is the front position at time $t = 0$.

porous medium with porosity and permeability varying in the horizontal direction. Under the conditions of validity of the Hele-Shaw analogy for power-law fluids, the solution to the problem is analogous to that of converging flow in a channel of varying gap thickness.

2. Converging flow in channel of variable cross-section

A viscous gravity current of a Ostwald-de Waele fluid (power-law, PL) (Ostwald 1929; Morrell & De Waele 1920) propagates in the negative x direction within a channel (or fracture or Hele-Shaw cell) of variable cross-section (see figure 1), starting at x_0 and reaching the origin $x = 0$ at a finite touch-down time t_c.

The PL model for a shear-thinning/thickening fluid reads in one dimension

$$\tau = \mu_0 |\dot{\gamma}|^{n-1}\dot{\gamma} \tag{2.1}$$

in terms of the tangential stress τ and of the strain rate $\dot{\gamma}$. The consistency index μ_0 represents a viscosity-like parameter, and the fluid behaviour index n controls the extent of shear-thinning ($n < 1$) or shear-thickening ($n > 1$); $n = 1$ corresponds to the Newtonian case. A slightly more complicated description using tensors is required for three dimensional flows; this general formulation is not reported here as a one-dimensional problem is considered. The fluid advances in a horizontal channel with a gap thickness varying as $b(x) = b_1x^k$ ($[b_1] = L^{1-k}$ and $0 < k < 1$), see figure 1, under the hypotheses of (i) hydrostatic pressure distribution; (ii) $\tau_{xy} \gg \tau_{xz}$ and negligible τ_{yz}, i.e. tangential stress acting on the plane of normal x along the cross direction y, is dominant with respect to tangential stress acting on the same plane in vertical direction z; no slip at the side wall at $y = \pm\, b/2$ and symmetry at $y = 0$; (iv) negligible surface tension and no fingering at the interface with the ambient fluid, and (v) inviscid ambient fluid. The lubrication approximation holds and the flow is one-dimensional along the x axis except near the origin, where also the capillary length is comparable to the gap thickness and τ_{xz} is comparable to τ_{xy}. The stream-wise horizontal velocity of the current averaged over the cross-section is

$$u(x,t) = -\mathrm{sgn}\left(\frac{\partial h}{\partial x}\right)\left(\frac{b_1x^k}{2}\right)^{(n+1)/n}\frac{n}{2n+1}\left(\frac{\Delta\rho\, g}{\mu_0}\right)^{1/n}\left|\frac{\partial h}{\partial x}\right|^{1/n}, \tag{2.2}$$

where $h(x,t)$ is the current depth, $\Delta\rho \equiv \rho_c - \rho_a$ is the density difference between the intruding current and the ambient fluid and g is gravity. The mass conservation reads

$$\frac{\partial h}{\partial t}+\frac{1}{x^k}\frac{\partial(x^k h u)}{\partial x}=0. \tag{2.3}$$

The boundary conditions are motivated by the singular points in the phase plane described later. We anticipate that the boundary conditions allowing a solution are as follows: for $t<t_c$ are $h=0$ for $x=x_f$ and $u=0$ for $x\to\infty$, where t_c is the touch-down time required by the front of the current to reach the origin of the channel; for $t>t_c$ are $u=0$ and $\partial h/\partial x=0$ for $x=0$; for $t=t_c$ a singularity is reached, which is then removed upon a proper reformulation of the dependent variables. The integral mass conservation, although not specifically involved in the sought self-similar solution of the second-kind, are important in numerical integration schemes; the most common representation corresponds to $V\propto t^{\sigma}$, where $\sigma=0$ is the lock-release of a finite and constant volume of fluid, $\sigma=1$ is the constant inflow rate, $0<\sigma<1$ is a waning and $\sigma>1$ is a waxing inflow rate, respectively.

A first-kind self-similar solution cannot be obtained and a second-kind self-similar approach is pursued introducing the phase-formalism with the adoption of the independent variables, x and t, as length and time scales, respectively, to render the governing equations dimensionless.

We let

$$u(x,t)=\frac{x}{t_r}U(x,t_r), \tag{2.4a}$$

$$h(x,t)=\left(\frac{2}{b_1}\right)^{n+1}\left(\frac{2n+1}{n}\right)^{n}\left(\frac{\mu_0}{\Delta\rho\, g}\right)\frac{x^{(n+1)(1-k)}}{t_r|t_r|^{n-1}}H(x,t_r), \tag{2.4b}$$

where H and U are dimensionless and $t_r=t_c-t$. $t_r>0$ represents the pre-closure phase, with the fluid advancing towards the origin of the channel; $t_r<0$ identifies the post-closure phase, with the fluid occupying the entire channel length, the fluid surface undergoing a progressive levelling and the front position being $x_f=0$. U is negative and H is positive in the pre-closure phase, and change sign during the post-closure phase since t_r becomes negative.

Substituting eqs.(2.4a–2.4b) into eqs.(2.2–2.3) yields

$$U\left|U\right|^{n-1}+(n+1)(1-k)H+x\frac{\partial H}{\partial x}=0, \tag{2.5a}$$

$$t_r\frac{\partial H}{\partial t_r}-nH-HU(n+2-nk)-x\frac{\partial HU}{\partial x}=0. \tag{2.5b}$$

We assume a similarity variable $\xi=xt_r^{-1}|t_r|^{1-\delta}$, where the exponent δ cannot be determined by using dimensional arguments and must be determined in a different way. Inserting the similarity variable into eqs.(2.5a–2.5b) gives

$$U\left|U\right|^{n-1}+\xi H'+(n+1)(1-k)H=0, \tag{2.6a}$$

$$\delta\xi H'+nH+\xi(HU)'+(n+2-nk)HU=0, \tag{2.6b}$$

where the prime indicates the derivative with respect to ξ and where the variable t_r does not appear. Eliminating ξ from the two equations results in

$$\begin{cases}\dfrac{\mathrm{d}H}{\mathrm{d}U}=\dfrac{H[(n+1)(1-k)H+U\left|U\right|^{n-1}]}{H[(k+1)U-(n+1)(1-k)\delta+n]-(U+\delta)U\left|U\right|^{n-1}}, & (2.7a)\\[2ex] \dfrac{\mathrm{d}\ln\xi}{\mathrm{d}H}=-\dfrac{1}{U\left|U\right|^{n-1}+(n+1)(1-k)H}. & (2.7b)\end{cases}$$

These two equations are a set of autonomous planar ODEs, with boundary conditions represented by points in the phase space. We notice that the similarity variable has been embedded in its logarithm, with $\mathrm{d}\,\xi/\xi \equiv \mathrm{d}(\ln\xi)$. We define as singular points the simultaneous zeros of numerator and denominator of eq.(2.7a), with a further singular point obtained by setting the denominator to infinity. Hence there are four singular points, namely

$$\begin{aligned}
&\mathrm{O} : (H, U) \equiv (0, 0),\\
&\mathrm{A} : (H, U) \equiv (0, -\delta),\\
&\mathrm{B} : (H, U) \equiv \left(\left[\frac{n}{2+n(1-k)}\right]^n \frac{1}{(n+1)(1-k)}, -\frac{n}{2+n(1-k)}\right),\\
&\mathrm{C} : (H, U) \equiv \left(-\infty, \frac{(n+1)(1-k)\delta - n}{k+1}\right).
\end{aligned}$$

In the phase plane a solution connects two points representing the boundary conditions. In this sense, the singular points are crucial because they are the candidates for the role of representatives of the boundary conditions, and the behaviour of the solution must be sought in the neighborhood of these singularities.

Point O corresponds to null velocity and height at $t_r = 0$ (and to $\xi \to \infty$); point A corresponds to the moving front where $h(x_f(t), t) = 0$, with x_f the front position and $x_f(t = 0) = x_0$ (and to $\xi = \xi_f$); point B has no specific clear meaning, and from an analytic point of view corresponds to the condition $\mathrm{d}^2H/\mathrm{d}U^2 \equiv \mathrm{d}H/\mathrm{d}U = 0$; point C is active during the post-closure levelling of the current, and represents the asymptotic flow condition (it also corresponds to $\xi = 0$). For $n = 1$ point B corresponds to the value given in Zheng *et al.* (2014) (where n in Zheng *et al.* 2014, corresponds to our k).

The expansion about point O, computed by assuming $H = \varpi U^\nu$, substituting in eq.(2.7a) and balancing the smaller order terms to calculate ϖ and ν, gives

$$U \approx -\left[\frac{\delta(1-k)(n+1) - n}{\delta}\right]^{1/n} H^{1/n}; \tag{2.8}$$

the expansion about point A, the front of the current, computed by assuming $H = \varpi(U + \delta)^\nu$, substituting in eq.(2.7a) and balancing the smaller order terms, yields

$$U \approx \left[\frac{(2+n-kn)\delta - n}{2\delta^n}\right]^{1/n} H - \delta; \tag{2.9}$$

the asymptotic expression for $H \to -\infty$ (point C) is computed by assuming $1/H = \varpi(1 - U/U_C)^\nu$, substituting in eq.(2.7a) and balancing the smaller order terms, and gives

$$U \approx U_C + \frac{U_C^{n+1}(U_C + \delta)}{U_C(k+1) + (n+1)(1-k)} \frac{1}{H}, \tag{2.10}$$

where U_C is the coordinate of the singular point C.

Given these properties of the singular points, we expect that the pre-closure phase is described by an integral curve joining A and O, the post-closure phase by a curve joining O and C.

Numerical integration with Mathematica (Wolfram Research, Inc. 2017) has been performed in the pre-closure time interval ($t < t_c$) by adopting eq.(2.7a), starting nearby the origin O and assuming that $U = -\epsilon$ with the local expansion for H given by eq.(2.8) in the form

$$H|_{-\epsilon} \approx \frac{\delta}{\delta(1-k)(n+1)-n}\epsilon^{n}, \tag{2.11}$$

with $\epsilon = 10^{-5}$, and computing $H(U)$ in the interval $U \in [-\delta, -\epsilon]$. An initial value of δ was chosen, with iterative modifications of this value and stop criterion when $H(-\delta) < 10^{-3}$. The computed eigenvalues, named critical eigenvalues δ_c, are listed in table A.1 of Appendix A.

Numerical integration in the post-closure interval ($t > t_c$) has been performed with the same equation (2.7*a*) used for the pre-closure interval, but starting nearby point C where $U = U_C - \epsilon$, with the expansion for H given by eq.(2.10) in the form

$$H|_{(U_C-\epsilon)} \approx -\frac{U_C^{n+1}(U_C+\delta_c)}{U_C(k+1)+(n+1)(1-k)}\epsilon^{-1}, \tag{2.12}$$

again with $\epsilon = 10^{-5}$, and computing $H(U)$ in the interval $U \in [\epsilon, U_C - \epsilon]$. No iteration was required since the value of δ_c was already known.

Figure 2 shows the phase portrait of eq.(2.7*a*) with the trajectories for the critical eigenvalue $\delta_c = 1.5836$ for $n = 0.5$ (a typical value for a shear-thinning fluid) and $k = 0.5$ (a fracture enlarging with the square root of the abscissa). Continuous and dashed curves describe the pre-closure and post-closure phases, respectively. Figure 3a shows the heteroclinic trajectories connecting: i) point A and point O (continuous curves, pre-closure) and ii) point O and point C (dashed curves, post-closure or levelling) for fixed $n = 0.5$ and increasing k values. For $k \to 1$ the variation of the current depth with U tends to zero near the front and to $-\infty$ near the origin, and $U_C \to 0$. Figure 3b shows the same curves but for fixed $k = 0.5$ and increasing values of the flow-behaviour index n. Figure 4 shows the eigenvalues as a function of k for different n. The asymptotic value for $k \to 1$ is $\delta_c \approx n/[(n+1)(1-k)]$ and corresponds to $U_C \to 0$. The Newtonian fluid ($n = 1$) shows the minimum eigenvalues for a given value of the width coefficient k. Relative differences between eigenvalues corresponding to different values of n are modest while $k \leqslant 0.7$, then increase rapidly, especially for very shear-thinning fluids. We observe that the eigenvalues are not monotonic with n, and are decreasing with n if $n < 1$, increasing if $n > 1$, see also the numerical values of δ_c in Table A.1. An increase in the eigenvalue results in a higher front velocity ($U_f = -\delta_c$). This seems to be the result of an interplay between rheology and channel geometry. Observing Figure 5a, it appears that the slope of the free surface current (i.e. the gradient pressure) for $\xi \to \xi_f$ increases with n. The front speed results from a balance between gradient pressure and flow resistance. For shear thinning fluids the reduction of resistance with n is more than the reduction of gradient pressure, and the nose of the current is faster for decreasing n; for shear-thickening fluids the increase of resistance is less than the increase of the gradient pressure, and again the nose of the current is faster for increasing n.

Once the function $H(U)$ has been computed, in order to evaluate the independent similarity variable ξ it is convenient to rewrite the l.h.s. eq.(2.7*b*) as $\mathrm{d}\ln(\xi)/\mathrm{d}U$ via the chain rule and the inverse function theorem using eq.(2.7*a*), and also to map the domain of varying size $\xi \in [\xi_f, \infty]$ into $\xi/\xi_f \in [1, \infty]$. The resulting differential equation

$$\frac{\mathrm{d}\ln\xi/\xi_f}{\mathrm{d}U} = -\frac{H}{H[(k+1)U-(n+1)(1-k)\delta_c+n]-(U+\delta_c)U\,|U|^{n-1}} \tag{2.13}$$

can be integrated in the range $U \in [-\delta_c, -\epsilon]$ starting from A, the front of the current,

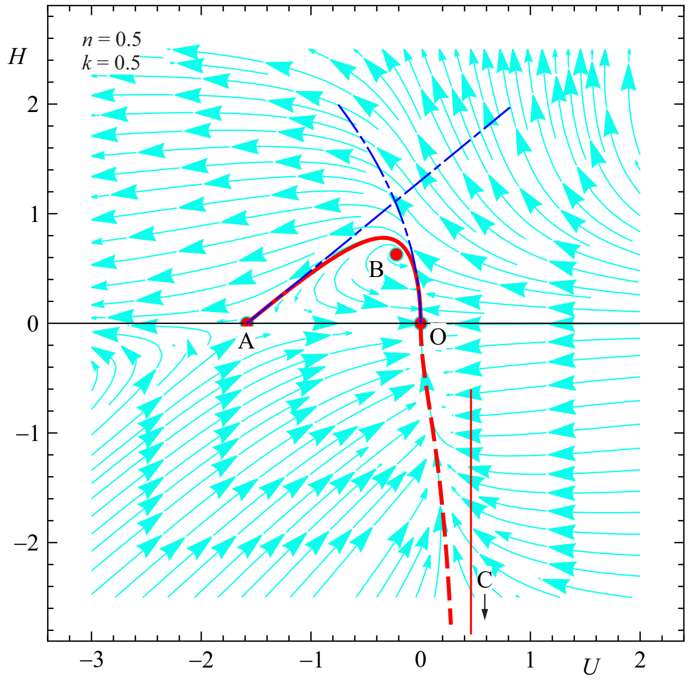

FIGURE 2. Converging gravity current in a fracture of gap thickness $b = b_1 x^k$. Phase portrait of (2.7a) for $n = 0.5$ (shear-thinning fluid) and $k = 0.5$, with $\delta_c = 1.5836$. The singular points are O : $(0, 0)$, A : $(0, -1.5836)$, B : $(0.6285, -0.2222)$, C : $(-\infty, 0.4585)$. The continuous curve refers to the pre-closure phase, the dashed curve refers to the post-closure (levelling) phase, the thin red vertical line indicates the asymptote in the levelling phase, the dash-dot blue curves are the approximate solutions about points O and A.

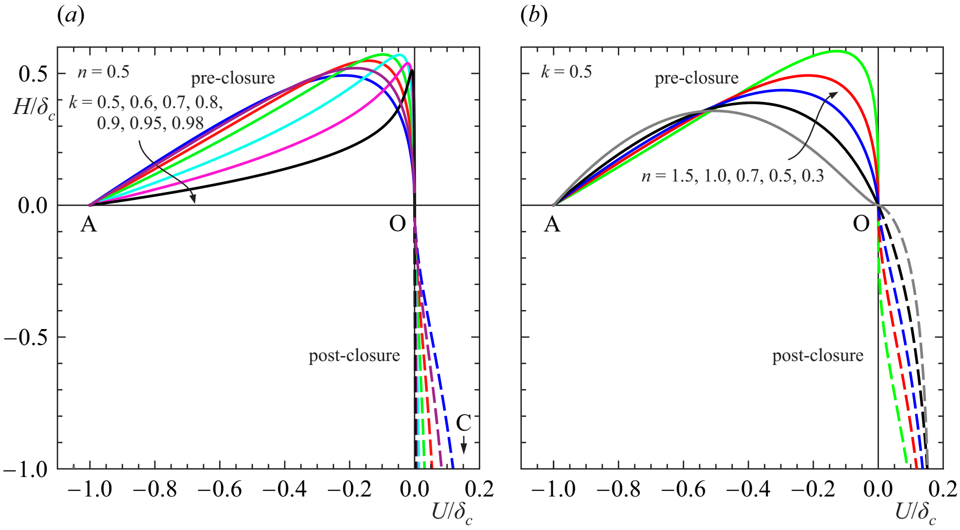

FIGURE 3. Converging gravity current in a channel of gap thickness $b = b_1 x^k$. Shape of the heteroclinic trajectories in rescaled coordinates for (a) $n = 0.5$ (shear-thinning fluid) as $k \to 1$; (b) $k = 0.5$ (a fracture enlarging with the square root of the abscissa) as n varies from 0.5 (shear-thinning) to 1 (Newtonian) and to 1.5 (shear-thickening). Continuous curves refer to pre-closure, dashed curves to post-closure (levelling) phase.

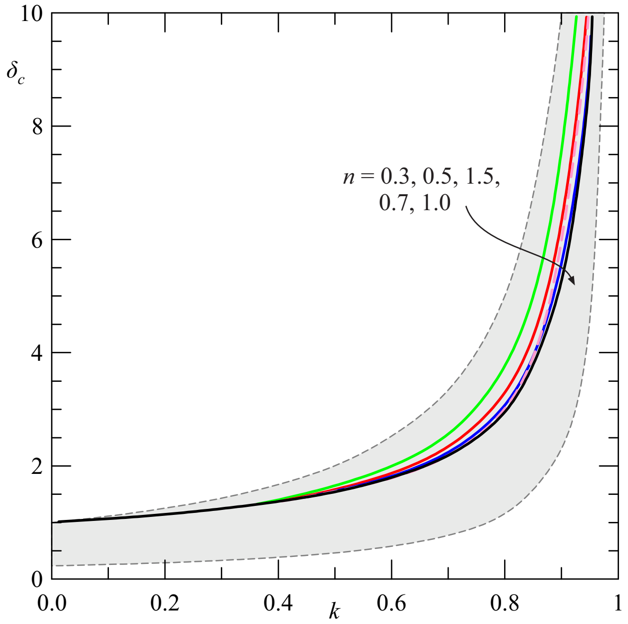

FIGURE 4. Converging gravity current in a channel of gap thickness $b = b_1 x^k$. Eigenvalues representing the exponent of the similarity variable $\xi = x/(t_c - t)^{\delta_c}$ for fluids with different flow behaviour index n. The dashed pink curve refers to a shear-thickening fluid with $n = 1.5$, the hatched area is limited by the upper boundary, $1/(1-k)$, and by the lower boundary, $n/[(n+1)(1-k)]$, for $n = 0.3$, of the critical eigenvalues.

with the boundary condition $\xi/\xi_f|_{U=-\delta_c} = 1$, equivalent to $\mathrm{d}\ln(\xi/\xi_f)|_{U=-\delta_c} = 0$. The origin O is reached for $U \to 0$ at $\xi/\xi_f \to \infty$.

Figure 5a shows the self-similar current shape profiles and the velocity profiles in the pre-closure phase, for $k = 0.5$ and different values of n. We notice that velocity profiles are almost coincident, while the shape of the current is markedly influenced by the flow behaviour index n, with a crest near the front more evident the more shear-thickening is the the fluid.

A similar approach is adopted for the post-closure phase, when the front of the current has reached the origin and a progressive levelling occurs. In this phase it is convenient to integrate eq.(2.7b) from point O, with $\ln \xi|_{H=-\epsilon} = -(\delta_c/n)\ln(\epsilon)$. For increasing H (in absolute value), the similarity variable $\xi \to 0$, the neighborhood of point C where $U \to U_C$. Figure 5b shows the current depth and velocity for different values of the fluid behaviour index n and for $k = 0.5$. The results for other values of the width exponent k are similar (not shown).

Inserting the expansion (2.8) near the origin O into eq.(2.7b) and solving the resulting differential equation, yields

$$H \approx K\xi^{-n/\delta_c}, \tag{2.14}$$

$$U \approx -\left[\frac{\delta_c(1-k)(n+1)-n}{\delta_c}\right]^{1/n} K^{1/n}\xi^{-1/\delta_c}. \tag{2.15}$$

Switching to dimensional variables gives

$$h(x) = \left(\frac{2}{b_1}\right)^{n+1}\left(\frac{2n+1}{n}\right)^{n}\left(\frac{\mu_0}{\Delta\rho\, g}\right) K x^{(n+1)(1-k)-n/\delta_c}, \tag{2.16}$$

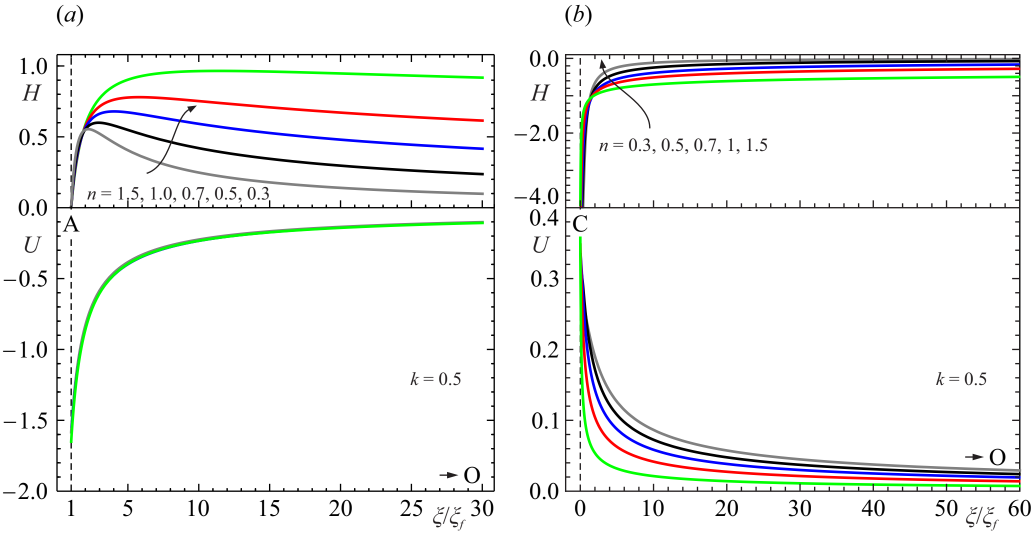

FIGURE 5. Converging gravity current in a channel of gap thickness $b = b_1 x^k$. Self-similar current shape profiles and velocity profiles for $k = 0.5$ (a fracture enlarging with the square root of the abscissa) and for $n = 0.3, 0.5, 0.7, 1.0, 1.5$ (*a*) in the pre-closure phase, and (*b*) in the post-closure phase.

$$u(x) \approx -\left[\frac{\delta_c(1-k)(n+1)-n}{\delta_c}\right]^{1/n} K^{1/n} x^{1-1/\delta_c}, \tag{2.17}$$

where K is a constant. Notably, eqs.(2.16–2.17) are time independent.

For $x \to \infty$ the depth of the current grows in the positive direction, hence $\mathrm{d}h/\mathrm{d}x > 0$ that in turn implies

$$\delta_c > \frac{n}{(n+1)(1-k)}, \tag{2.18}$$

which also satisfies the condition of a negative velocity. The minimum value of δ_c grows with n and k, and tends to infinity for $k \to 1$ (a linearly expanding fracture).

In a similar manner, inserting the expansion (2.10) near C into eq.(2.7*b*) and solving the differential equation, yields

$$H \propto \xi|\xi|^{-(n+1)(1-k)-1}, \tag{2.19}$$

or

$$h \propto t_r|t_r|^{\delta_c(n+1)(1-k)-n-1}, \tag{2.20}$$

in dimensional variables. Eq.(2.20) is independent on x and represents the levelling process near $x = 0$.

The condition of a time increasing h during levelling, $\mathrm{d}h/\mathrm{d}t > 0$, equivalent to $\mathrm{d}h/\mathrm{d}t_r < 0$, requires that

$$\frac{\mathrm{d}h}{\mathrm{d}t_r} \propto [\delta_c(n+1)(1-k)-n]t_r|t_r|^{\delta_c(n+1)(1-k)-n-2} < 0 \to \delta_c > \frac{n}{(n+1)(1-k)}, \tag{2.21}$$

coincident with the condition (2.18). Imposing that the levelling process vanishes in time, i.e.

$$\lim_{t_r \to -\infty} \frac{\mathrm{d}h}{\mathrm{d}t_r} = 0, \tag{2.22}$$

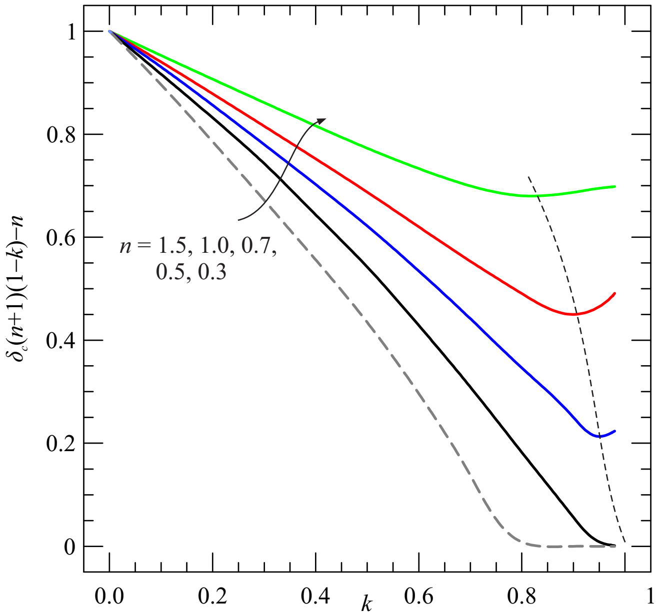

FIGURE 6. Converging gravity current in a channel of gap thickness $b = b_1 x^k$. Time exponent of the growth rate of the depth of the current at the origin during levelling (see eq.(2.20)as a function of k for fluids with different flow behaviour index n ranging from shear-thinning to shear-thickening. The dashed thin curve indicates the minimum for each n value.

requires that

$$\delta_c < \frac{1}{1-k}. \tag{2.23}$$

In conclusion, the critical eigenvalue is bounded above and below, i.e.

$$\frac{n}{(n+1)(1-k)} < \delta_c < \frac{1}{1-k}, \tag{2.24}$$

with the two bounds collapsing to $1/(1-k) = \delta_c$ for an infinitely shear-thickening fluid or $n \to \infty$. Note that the upper bound is independent on the fluid nature. The lower bound for $n = 1$ coincides with the result by Zheng *et al.* (2014) (their n is our k). For $k \to 0$ (constant gap thickness) and $n \to \infty$, it results $\delta_c = 1$.

Due to these constraints on the eigenvalues, the time exponent of the depth growth rate at the origin during levelling, defined in eq.(2.20), varies in the range $[0, 1]$, see figure 6 where its value is depicted versus k for different values of the flow behaviour index n. As the parameter k describing the growth rate of the fracture gap increases, the same exponent decreases up to a minimum value depending on the fluid rheology, then modestly increases; this is so only for shear-thinning fluids, while the exponent for shear-thickening and Newtonian fluids reaches a minimum and remains approximately constant. The minimum value of the exponent in eq.(2.20) is reached for $k = 0.75 - 1$. Finally, the exponent increases as the flow behaviour index decreases from shear-thickening to shear-thinning rheology.

In Appendix B we consider a related problem: the propagation of a plane gravity current of profile $h(x,t)$ toward the origin of the coordinate system in an heterogeneous porous medium with spatially variable permeability and porosity. If both quantities exhibit a power-law variation in the streamwise direction x, a formal analogy can be established between two domains, the porous medium and the Hele-Shaw cell or channel of

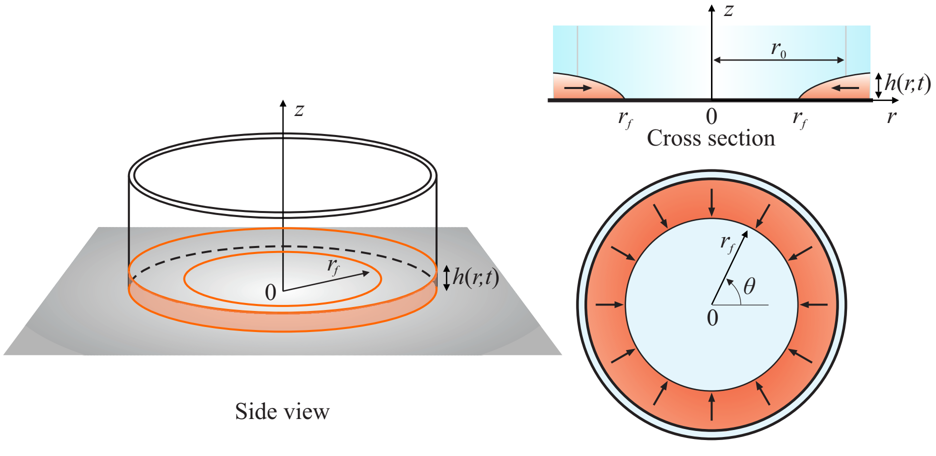

Cross section

Side view

Top view

FIGURE 7. Radial converging flow: a gravity current in viscous-buoyancy balance propagates towards the origin. r_f is the instantaneous front position, r_0 is the front position at time $t = 0$.

variable gap thickness. The analogy is subject to constraints in the values of parameters describing the heterogeneity as detailed in Appendix B.

3. Converging axisymmetric flow

We consider the converging flow of a cylindrical gravity current as shown in figure 7: the current propagates towards the origin of a cylindrical coordinate system. We assume again: (i) the current to be thin, allowing a hydrostatic pressure distribution, (ii) τ_{rz} to be the dominant shear, with negligible contributions by $\tau_{r\theta}$ and $\tau_{\theta z}$; and (iii) no surface tension effects and no fingering at the interface with the ambient fluid; (iv) inviscid ambient fluid. Gravity is the driving force balanced by viscous forces. In the limits of lubrication model, the vertically averaged horizontal velocity in the radial direction, calculated by imposing the no slip condition $u = 0$ for $z = 0$ and a zero tangential stress at the interface with the ambient fluid, corresponding to $\partial u/\partial x = 0$ for $z = h$, is

$$u(r,t) = -\mathrm{sgn}\left(\frac{\partial h}{\partial r}\right) h^{(n+1)/n} \frac{n}{2n+1} \left(\frac{\Delta\rho\, g}{\mu_0}\right)^{1/n} \left|\frac{\partial h}{\partial r}\right|^{1/n}, \tag{3.1}$$

and mass conservation reads

$$\frac{\partial h}{\partial t} + \frac{1}{r}\frac{\partial(ruh)}{\partial r} = 0. \tag{3.2}$$

Again, in a general approach we should specify the initial and boundary conditions, but as already discussed in §2, the boundary conditions are motivated by the singular points in the phase plane.

The dependent variables u and h are rendered non dimensional as follows:

$$u(r,t) = \frac{r}{t_r} U(r,t_r), \tag{3.3a}$$

$$h(r,t) = \left(\frac{2n+1}{n}\right)^{n/(n+2)} \left(\frac{\mu_0}{\Delta\rho\, g}\right)^{1/(n+2)} \frac{r^{(n+1)/(n+2)}}{t_r |t_r|^{-2/(n+2)}} H(r,t_r). \tag{3.3b}$$

Then the similarity independent variable $\xi = r t_r^{-1} |t_r|^{1-\delta}$ is introduced, where δ is the yet unknown eigenvalue. With the same approach described for converging flow in a horizontal fracture, eqs.(3.1–3.2) are rearranged to obtain

$$\begin{cases} \dfrac{\mathrm{d}U}{\mathrm{d}H} = \dfrac{H|H|^{n+1}[2(n+2)U-(n+1)\delta+n]-(U+\delta)(n+2)U\,|U|^{n-1}}{H[(n+1)H|H|^{n+1}+(n+2)U\,|U|^{n-1}]}, & (3.4a) \\ \dfrac{\mathrm{d}\ln\xi}{\mathrm{d}H} = -\dfrac{n+2}{(n+2)H^{-1}|H|^{-n}U\,|U|^{n-1}+(n+1)H}. & (3.4b) \end{cases}$$

The singular points are

$$\begin{aligned} &\mathrm{O}:(H,U)\equiv(0,0),\\ &\mathrm{A}:(H,U)\equiv(0,-\delta),\\ &\mathrm{B}:(H,U)\equiv\left(\left[\frac{n+2}{n+1}\right]^{1/(n+2)}\left[\frac{n}{5+3n}\right]^{n/(n+2)},-\frac{n}{5+3n}\right),\\ &\mathrm{C}:(H,U)\equiv\left(-\infty,\frac{(n+1)\delta-n}{2(n+2)}\right), \end{aligned}$$

and have the same meaning of the points described for converging fracture flow.

The case $n=1$ refers to a Newtonian fluid, and eqs.(3.4*a*–3.4*b*) become

$$\begin{cases} \dfrac{\mathrm{d}U}{\mathrm{d}H} = \dfrac{H^3[6U-2\delta+1]-3U(U+\delta)}{H[2H^3+3U]}, & (3.5a) \\ \dfrac{\mathrm{d}\ln\xi}{\mathrm{d}H} = -\dfrac{3H^2}{3U+2H^3}, & (3.5b) \end{cases}$$

and the singular points are

$$\begin{aligned} &\mathrm{O}:(H,U)\equiv(0,0),\\ &\mathrm{A}:(H,U)\equiv(0,-\delta),\\ &\mathrm{B}:(H,U)\equiv\left(\left[\frac{3}{16}\right]^{1/3},-\frac{1}{8}\right),\\ &\mathrm{C}:(H,U)\equiv\left(-\infty,\frac{2\delta-1}{6}\right), \end{aligned}$$

corresponding to the differential problem in Diez *et al.* (1992*b*) with a different definition of the variables. The results are equivalent to those reported in McCue *et al.* (2019), where a slightly different approach and a broader perspective is adopted, with an improved clarity of the various steps. See also Gratton & Perazzo (2010).

Numerical integration of the pre-closure phase starts with a first tentative value of δ and moving from the origin O ($\xi\to\infty$), where $H\to 0$ and the solution for U is approximated by

$$U \approx -H|H|^{2/n}\left[\frac{(n+1)\delta-n}{(n+2)\delta}\right]^{1/n}. \qquad (3.6)$$

Upon successive iterations with changes of the δ value, the integral curve reaches exactly point A ($\xi=\xi_f$), the front of the gravity current, where $H\to 0$ and the approximate solution for U is

$$U \approx -\delta + \frac{2}{(n+3)\delta^{n-1}}H|H|^{n+1}. \qquad (3.7)$$

The value of δ that allows the integral curve to reach A from O is the critical eigenvalue δ_c.

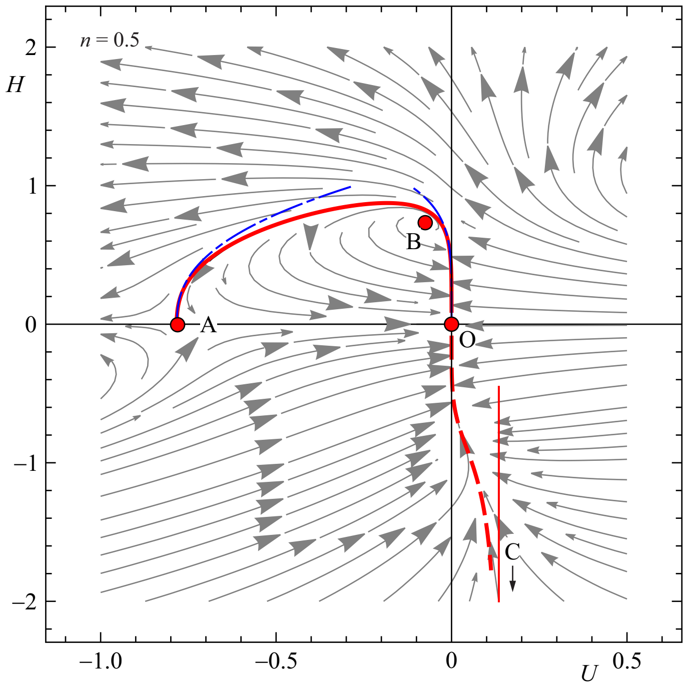

FIGURE 8. Converging radial gravity current. Phase portrait of (3.4*a*) for $n = 0.5$ (shear-thinning fluid), $\delta_c = 0.78261$. The continuous curve refers to the pre-closure phase, the dashed curve refers to the post-closure (levelling) phase, the thin red vertical line indicates the asymptote in the levelling phase, the dash-dot blue curves are the approximate solutions about points O and A.

Numerical integration of the post-closure phase starts about point C, where $H \to -\infty$ (and $\xi \to 0$) and where the approximate solution for U is

$$U \approx U_C + \frac{(3+n)(n+2)}{U_C^n\,[U_C + (n+2)\delta_c]}\,\frac{1}{H|H|^{n+1}}, \tag{3.8}$$

and the integral curve reaches point O ($\xi \to \infty$), where the approximate solution is (3.6). In this second integration, iterations are not necessary since δ_c is already known. The expansion about the singular points O, A and C has been obtained in the same way as that reported for the differential problem describing the gravity current in a converging channels, see 2.

Figure 8 shows the phase portrait for a shear-thinning fluid with $n = 0.5$, with the integral curves for the pre- and post-closure phases, corresponding to an eigenvalue $\delta_c = 0.78261$. The eigenvalues for different values of n are listed in table A.2 of Appendix A and are shown in figure 9, where a shear-thinning behaviour is accompanied by higher δ_c, although the variability is quite modest; the corresponding integral curves are depicted in figure 10a, followed by the shape profiles and velocity profiles in the pre-closure phase in figure 10b. No specific trend is observed, although the thickness of the current immediately behind the front is larger for more shear-thinning fluids. The horizontal velocity is almost indistinguishable for currents with different value of the fluid behaviour index. The results for the eigenvalues coincide with those shown in Figure 1 in Gratton & Perazzo (2010), after converting the horizontal axis with their λ equal to $1/n$ in the notation of the present research.

The behaviour of the integral curves approaching O can be obtained by expanding

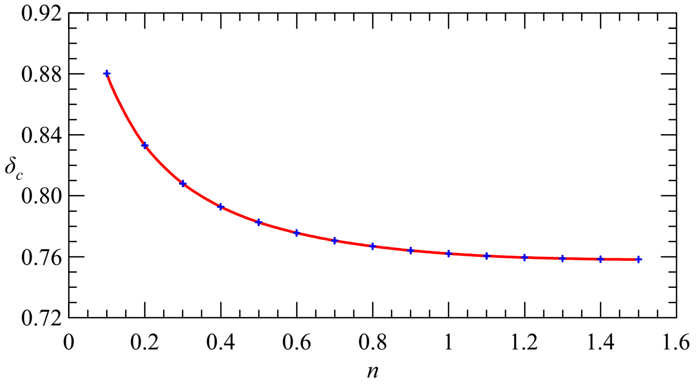

FIGURE 9. Converging radial gravity current. Eigenvalues representing the exponent of the similarity variable $\xi = x/(t_c - t)^{\delta}$ for axisymmetric flow towards the origin for fluids with different flow behaviour index n.

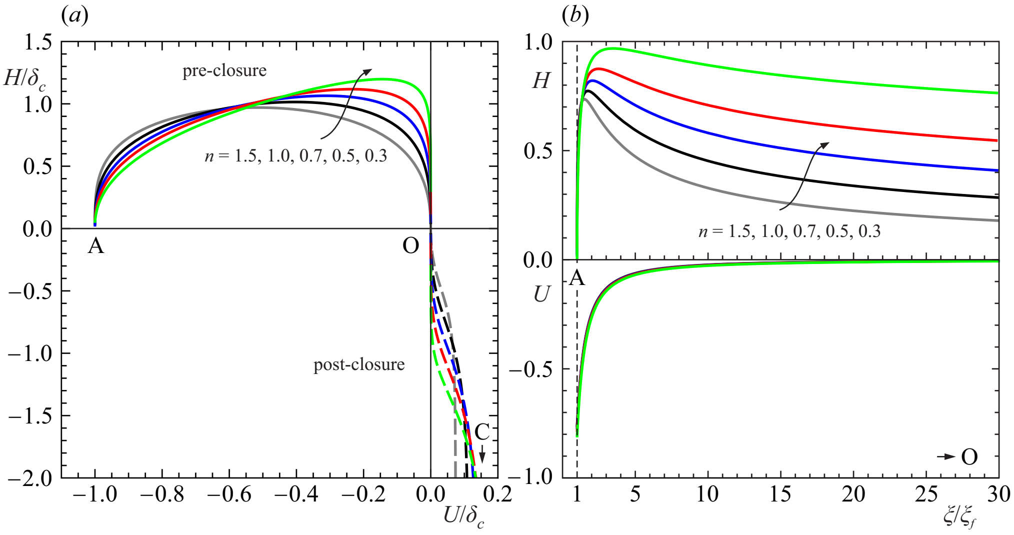

FIGURE 10. Converging radial gravity current. (a) Shape of the heteroclinic trajectories in the pre-closure (continuous curves) and post-closure (dashed curves) phase, and (b) shape profiles and velocity profiles in the pre-closure phase as n varies from 0.5 (shear-thinning) to 1 (Newtonian) and to 1.5 (shear-thickening).

$H = a_0\xi^b + a_1\xi^{b+1} + \ldots$. Then introducing the approximation (3.6) in eq.(3.4b) and balancing yields

$$H = K\xi^{-n/[\delta_c(n+2)]}, \tag{3.9}$$

$$U = -K^{(2+n)/n}\left[\frac{(n+1)\delta_c - n}{(n+2)\delta_c}\right]^{1/n}\xi^{-1/\delta_c}, \tag{3.10}$$

where K is a constant. Switching to dimensional variables, one obtains for the current depth and velocity

$$h(r) = \left(\frac{2n+1}{n}\right)^{\frac{n}{n+2}}\left(\frac{\mu_0}{\delta_c \rho\, g}\right)^{\frac{1}{n+2}} K r^{\frac{(n+1)\delta_c - n}{(n+2)\delta_c}}, \tag{3.11}$$

$$u(r) = -K^{(2+n)/n}\left[\frac{(n+1)\delta_c - n}{(n+2)\delta_c}\right]^{1/n} r^{(\delta_c-1)/\delta_c}, \tag{3.12}$$

that are time-independent. For $r \to \infty$ the depth of the current grows in the positive direction, hence $\mathrm{d}h/\mathrm{d}r > 0$ that in turn implies $\delta_c > n/(n+1)$, which also ensures a negative velocity.

A similar analysis can be conducted to describe the post-closure phase, with results similar to those obtained for converging flow in a horizontal fracture.

4. The experimental validation

4.1. *The experimental setup*

Three different experimental setups were developed in the Laboratory of Hydraulics of the University of Parma in order to validate the theoretical models.

The first setup consists of a tank to reproduce the propagation of gravity currents in converging channel flow. The channel consists of two rectangular plates, 150 cm long and 20 cm high, with a front wall made of transparent plastic for an easy visualization, while the back wall is made of yellow polyvinyl chloride (PVC) machined with a computerized numerical control machine; the gap thickness is $b(x) = b_1\, x^{0.6}$, where x is the abscissa with origin at the corner, as shown in figure 11; $b_1 = 0.01176$ m$^{0.4}$ and the width of the channel at $x = 150$ cm equals 1.5 cm. Lock release gravity currents were generated with different lengths of the lock, equal to $12, 14, 20, 30$ cm. One experiment was performed with a different boundary condition of given flux, in order to check the sensitivity of the solution to the inflow mode. A similar setup was adopted in Zheng *et al.* (2014) and also documented in Ghodgaonkar (2019), with a length of 75 cm. With this setup, the heavy fluid was Newtonian or non-Newtonian power-law shear-thinning, while the ambient fluid was always air.

A second series of experiments reproduced radial converging gravity currents and was carried out in a transparent plastic cell shaped as a circular sector (a wedge) with an angle at the centre $\beta = 12°$, a radius $R = 75$ cm and a height of $h = 18$ cm. The front, side and top view are shown in figure 12a-c. The front vertical wall is rigidly attached to the bottom, while the back wall is removable. At a distance $r_0 = 60$ cm a vertical gate is inserted in order to separate the heavy fluid in the upstream lock from the light ambient fluid in the downstream chamber. Three clamps are applied on top of the tank in order to push the walls against the bottom and prevent any leakage. Figure 12d is a picture of the experimental apparatus.

A third set of experiments for radial converging gravity currents was conducted in a fully metallic cylinder with an inner radius of $R_2 = 30$ cm. A smaller cylinder with an external radius $R_1 = 19.5$ cm is positioned concentrically to the prior one and pushed against the glass bottom (a soft rubber sealing gasket is present) in order to create an annular lock with a gap $\Delta R = R_2 - R_1 = 10.5$ cm. Particular attention was paid to the levelling of the base of the apparatus, so as to prevent asymmetries due to the gravitational force. An electronic level is used to this purpose, with an accuracy of 0.1°. The annulus is filled with dense fluid up to a depth of $h_0 = 3.3 - 4.5$ cm. The inner cylinder is filled with light ambient fluid. At the beginning of the experiments, the inner cylinder is lifted up to a known height $h < h_0$. A similar setup was used in Diez *et al.* (1992*b*), with radius of the external/internal cylinder of 20 and 5 cm, respectively.

For the currents in converging channel flow (setup #1), the Newtonian fluids were prepared with glycerol, while the non-Newtonian fluids were prepared with (i) a mixture of water (95% vol.), glycerol (5% vol.) and carboxymethyl cellulose (CMC, 2% by weight),

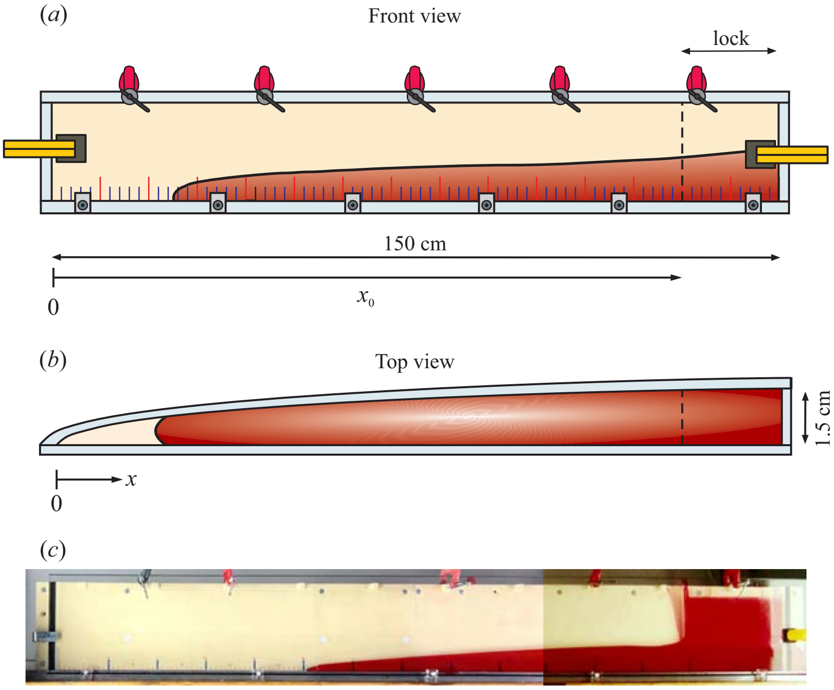

FIGURE 11. Experimental setup #1: tank with a gap thickness of $b_1\, x^{0.6}$. (*a*) Front view; (*b*) top view; (*c*) a photo during one of the tests; the lock is almost empty but a thin layer of fluid still adheres to the transparent wall, marking the volume occupied by the fluid in the lock before lifting the gate.

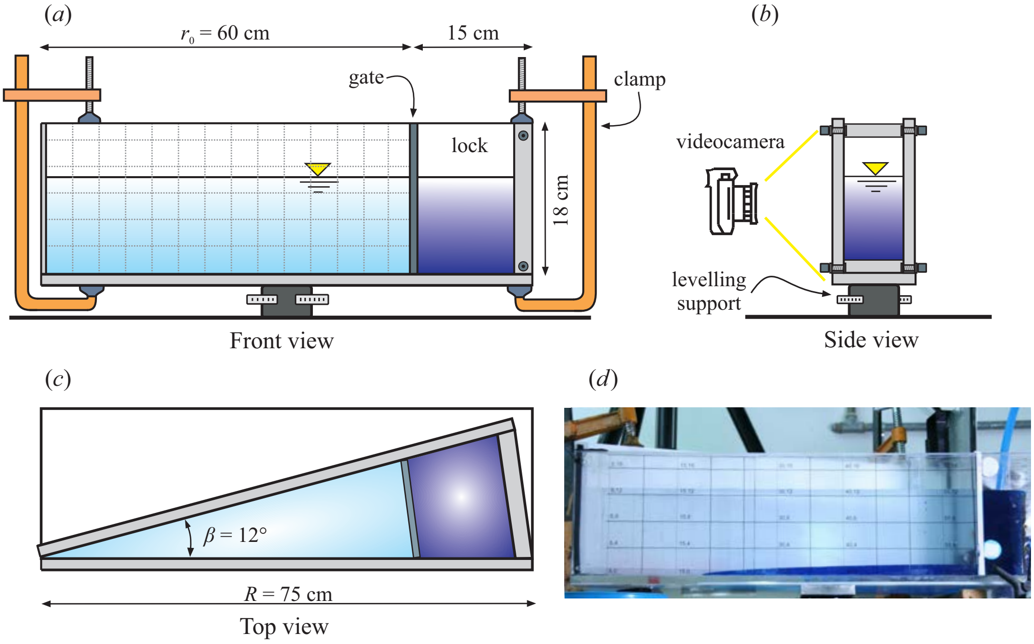

FIGURE 12. Experimental setup #2: circular sector cell with an angle at the centre $\beta = 12°$. (*a*) Front view; (*b*) lateral view and (*c*) top view. (*d*) Snapshot of the tank.

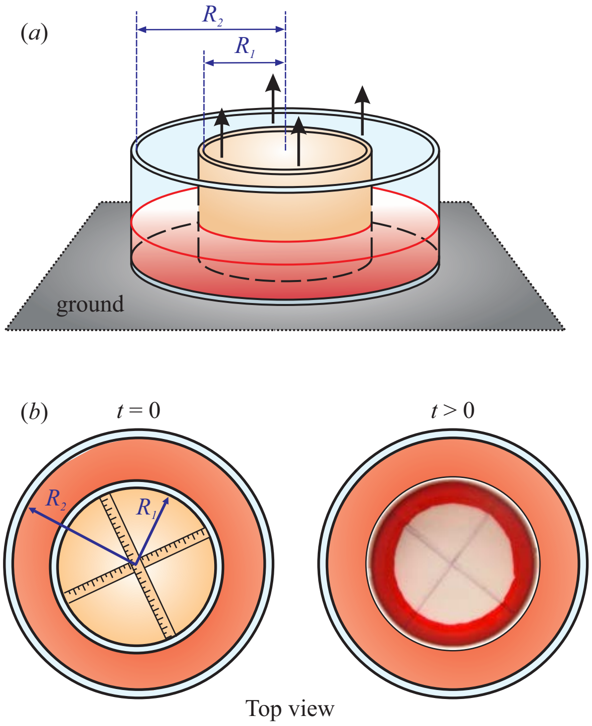

FIGURE 13. Experimental setup #3: radial symmetric cell. (*a*) Front view; (*b*) top view at $t = 0$, before the lift of the inner cylinder (sketch), and for $t > 0$, after the lift of the inner cylinder (photo).

or a (ii) a mixture of water (40% vol.), glycerol (60% vol.) and E415 (0.1% by weight). All the non-Newtonian fluids have power-law, shear-thinning rheology.

For the radial converging currents (setups $\#2-3$), the Newtonian fluids were prepared with either glycerol or a mixture of glycerol, salt and water, and non-Newtonian fluids with a mixture of water (60% vol.), glycerol (40% vol.) and Xanthan Gum (E415, 0.25% by weight). The light ambient fluid is water or a mixture of water, salt and glycerol with a density slightly less than the current fluid. The combination of different ambient fluids and intruding fluids was required in order to guarantee the viscous regime, with negligible inertial effects, and to increase the duration of the experiments for an accurate estimation of t_c. Aniline water color was finally added to the denser fluid for an easy visualization of the propagating current.

The rheology was measured by the parallel plate twin-driver MCR702 rheometer by Anton Paar, at a temperature of $\Theta = 25 - 27°$, equal to the ambient temperature during the experiments. Several different tests were performed in order to evaluate the fluid behaviour index and consistency index for non-Newtonian fluids, and the dynamic viscosity of Newtonian fluids. Figure 14 shows the experimental shear-stress/shear-rate curves for two different shear-thinning fluids. The limited range of shear-rate is dictated by the evidence that, except at the early stage of the current propagation, after the gate lift, the average shear-rate is quite modest. The estimated accuracy is $\Delta n/n \leqslant 4\%$ and $\Delta \mu_0/\mu_0 \leqslant 6\%$. The mass density of the fluids was measured by a hydrometer (STV350023 Salmoraghi), and by the DMA 5000 by Anton Paar, with an accuracy of $\Delta\rho/\rho_0 \leqslant 0.1\%$.

The profiles of the advancing current after the lift of the gate, are recorded by either a high-resolution video camera (Canon Legria 1920 × 1080 pixels) operating at 25 frames

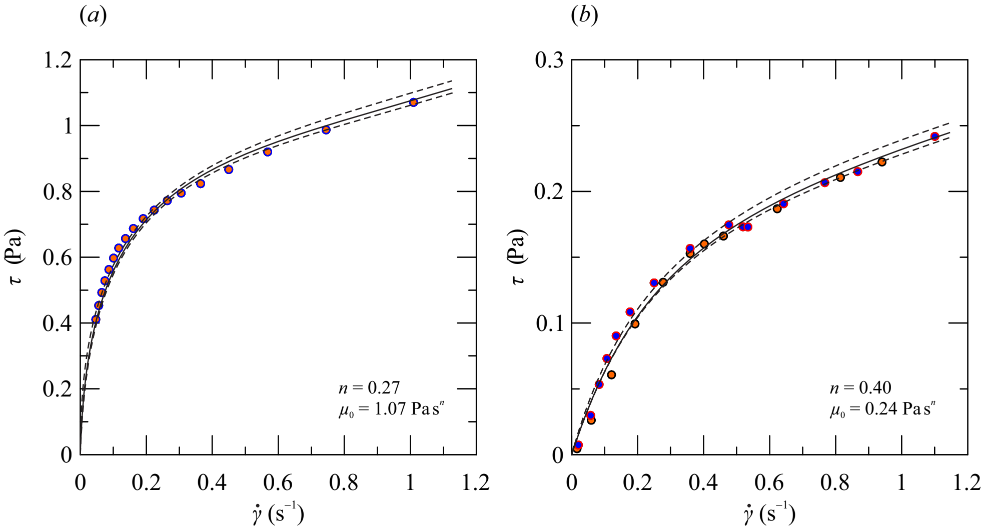

FIGURE 14. Experimental rheometry of two shear-thinning fluids. (*a*) Mixture of water, NaCl and Xanthan Gum, $\Theta = 27°\mathrm{C}$; (*b*) mixture of of water, NaCl and Xanthan Gum, with two series of measurements to check repeatability, $\Theta = 25°\mathrm{C}$. The solid curves are the power-law interpolation and the dashed curves are the 95% confidence limits.

per second (fps), or an iPhone 4K video camera working at 30 fps. For some experiments both videos were used in order to capture the whole profile of the current with an adequate resolution, see figure 11c where the panoramic image results from two frames extracted from two synoptic videos. The frames extracted from the video are post-processed using a Matlab code that converts pixels into metric coordinates. This conversion is possible thanks to a square grid attached onto the inner side of the front vertical wall, which allows compensation of the optical distortion. The overall accuracy in detecting the position of the nose and the profile of the current is approximately 0.1 cm, while the accuracy in measuring time is negligible ($1/50 - 1/60$ s).

Figure 15 shows a sequence of snapshots for one of the experiments in lock-release, Exp. 11, with both pre- and post-closure instants. After closure, the effect of capillarity near the origin is evident, with an increase in the level compared to the average value observed far from the origin. Local level for post-closure analysis was obtained correcting data for capillarity uprise.

4.2. *The experiments*

The parameters of the experiments are listed in table 1; 10 experiments were performed in the converging channel and 11 experiments in radial geometry, either in the 12° sector or in the full circle configuration. The theory assumes the dominance of viscous and buoyancy forces over inertia. The Reynolds number for channel flow can be expressed as ratio between the inertial and viscous forces per unit volume,

$$F_i \sim \Delta\rho \frac{u^2}{L},\ F_v \sim \mu_0 \frac{u^n}{L^{n+1}}, \rightarrow \mathrm{Re} = \frac{\Delta\rho\, u^{2-n} L^n}{\mu_0}, \tag{4.1}$$

where L is a length scale, taken to be equal to the channel maximum width $L = b_1 x_0^k$. The velocity scale can be assumed equal to x_0/t_c, hence

$$\mathrm{Re} = \frac{\Delta\rho\, x_0^{2-n+k} b_1}{\mu_0 t_c^{2-n}}. \tag{4.2}$$

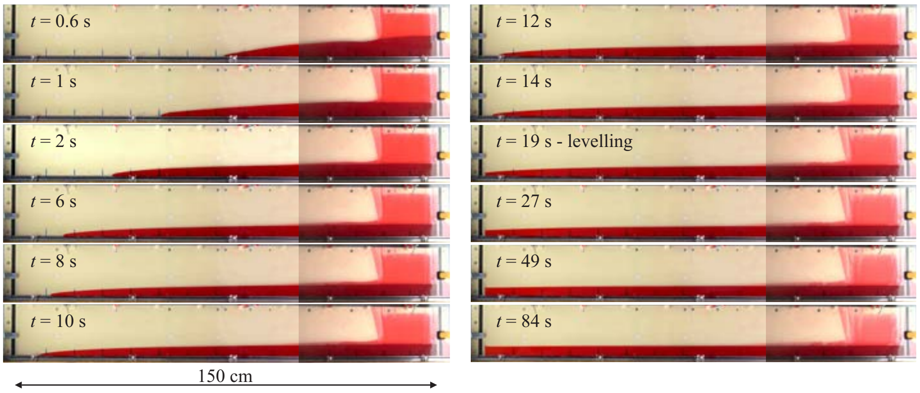

FIGURE 15. Time-lapse of the current profile for Exp. 11 in a channel of varying gap thickness. Closure is at $t_c = 16.4\,\mathrm{s}$, then levelling starts.

For radial gravity currents a similar analysis brings to a Reynolds number defined as

$$\mathrm{Re} = \frac{\Delta\rho\, u^{2-n} h^{n+1}}{\mu_o R}, \quad \text{with} \quad u \sim \left(\frac{\Delta\rho\, g}{\mu_0}\right)^{1/n} \frac{h^{(n+2)/n}}{R^{1/n}}, \tag{4.3}$$

hence

$$\mathrm{Re} = \left(\frac{\Delta\rho}{\mu_0}\right)^{2/n} g^{(2-n)/n} \frac{h^{(n+4)/n}}{R^{2/n}}. \tag{4.4}$$

The values of Reynolds number listed in the last column of table 1 refer to the initial stage of the current propagation; for channel flow $\mathrm{Re} < 1$ and for radial flow $\mathrm{Re} \ll 1$, with only one test initially characterized by $\mathrm{Re} \approx 0.8$. In the other tests, inertial effects are negligible since the very beginning, and the viscous balance dominates the advancement of the currents at all stages.

Figure 16 shows the time series of the front position for the experiments in converging channel flow. The experiments are separated in two groups, namely Newtonian and shear-thinning gravity currents. For the former tests the theoretical eigenvalue is $\delta_c = 1.787$ and the corresponding trajectory is fairly well followed by the experiments. Similar experiments were conducted in Zheng *et al.* (2014) in channels with different width exponent k, although only in lock-release mode. In the present Newtonian subset, four tests are in lock-release mode, while Exp. 1 is a constant influx experiment. The results indicate that in lock-release mode the current requires a much longer time to forget the initial condition and to reach self-similarity, whereas with a constant influx the current evolves rather quickly to reach the intermediate asymptotic regime of self-similarity. The different lengths of the locks do not influence significantly the current propagation in the far field. The grey symbols are considered outliers attributed to several disturbances and interferences, like capillarity and three dimensionality of the flow field not modelled in the theory. The Exp. 3 and 5 are a repetition with the same fluid and under the same conditions, to get an estimate of the repeatability and uncertainty.

For the non-Newtonian fluid experiments the fluid behaviour index ranges from 0.54 to 0.90, and the consistency index ranges from 0.42 to $2.63\,\mathrm{Pa\,s}^n$. The two straight lines in figure 16 correspond to extreme values of $\delta_c \approx 1.79$ and ≈ 1.85. Again the experimental results, all in lock-release mode, adequately follow the theory, reaching the self-similar regime although the differences with the value of n cannot be appreciated. Essentially, the long tank favours the evolution of the current with enough space to forget the inlet

Exp.	geom.	inflow condition	h, h_0 (cm)	a (cm)	lock length (cm)	r_0, x_0 (cm)	n	μ_0 ($\mathrm{Pa\,s}^n$)	ρ_c ($\mathrm{kg\,m^{-3}}$)	ρ_a ($\mathrm{kg\,m^{-3}}$)	t_c (s)	Re ($\times 10^{-3}$)
1	c	c-Q	-	-	-	150	1	1.10	1250	1.2	298	85
2	c	l-r	16.0	-	14	136	1	0.84	1250	1.2	350	81
3	c	l-r	16.0	-	20	130	1	1.10	1250	1.2	206	98
4	c	l-r	16.0	-	30	120	1	1.10	1250	1.2	126	141
5	c	l-r	16.0	-	20	130	1	1.10	1250	1.2	229	89
6	c	l-r	16.0	-	20	130	0.87	2.63	1022	1.2	670	4.6
7	c	l-r	16.0	-	30	120	0.87	2.63	1022	1.2	406	7.1
8	c	l-r	16.0	-	12	138	0.54	0.42	1070	1.2	80	94
9	c	l-r	16.0	-	14	136	0.90	1.74	1022	1.2	635	9.6
10	c	l-r	16.0	-	20	130	0.54	0.42	1070	1.2	28	387
11	c	l-r	16.0	-	20	130	0.54	0.42	1070	1.2	16.4	848
12	r12	c-h	9.2	1.4	15	60	1	0.11	1240	1210	237	6.0
13	r12	c-h	9.2	2.0	15	60	1	0.08	1241	1210	31	10
14	r12	c-h	9.2	2.0	15	60	1	0.13	1247	1220	56	3.4
15	r360	l-r	4.5	1.0	10.5	19.5	1	1.10	1260	1200	492	2.5
16	r360	l-r	4.5	2.0	10.5	19.5	1	1.10	1250	1190	22	2.5
17	r12	c-h	9.2	3.0	15	60	0.29	0.58	1031	1000	5233	0.0008
18	r12	c-h	9.2	2.2	15	60	0.40	0.24	1045	1000	58	4.2
19	r12	c-h	9.2	2.0	15	60	0.27	1.07	1024	1000	826	0.0001
20	r12	c-h	9.2	2.0	15	60	0.28	1.05	1036	1000	204	0.0001
21	r360	l-r	3.5	1.5	10.5	19.5	0.63	0.15	1032	1000	600	226

TABLE 1. Parameters for the experiments on converging flow in a channel of variable thickness and in radial geometry. The second column indicates the geometry of the flow field, where "c" stands for channel and where "r12" and "r360" stand for radial geometry with an angle at the centre of 12° and 360°, respectively; "c-Q", "l-r", "c-h" stand for constant inflow rate, lock-release and constant head; h and h_0 are the constant head or the initial depth in the lock; a is the height of the slot at the bottom of the gate; r_0, x_0 is the initial position of the front of the current in radial geometry and in the channel; n and μ_0 are the fluid behaviour index and the consistency index (the viscosity for Newtonian fluids) of the current fluid, respectively; ρ_c, ρ_a are the current/ambient fluid density and t_c is the touch-down time; Re is the Reynolds number according to the expressions (4.2–4.4), where an average value $h = 2\,\mathrm{cm}$ is assumed for radial gravity currents.

and initial conditions and before reaching the proximity of the origin, where capillarity renders the theoretical model invalid.

A comparison of the shape of the current with the experiments is reported for two experiments, with Newtonian and power-law fluids, respectively. A main variable in checking the validity of the model is the time position of the front of the current. We expect that $x_f(t) \propto t_r^{\delta_c}$, hence

$$\frac{x_f(t)}{x_0} = \alpha \left(\frac{t_r}{t_c} \right)^{\delta_c}, \tag{4.5}$$

where the dimensionless coefficient α is the intercept of the straight interpolating line in a diagram $x_f/x_0 - t_r/t_c$ drawn in logarithmic scale. It also results

$$\xi_f = \frac{\alpha x_0}{t_c^{\delta_c}}, \tag{4.6}$$

which is a constant for each experiment. The value of α is obtained by interpolating the experimental front-position of the advancing current in pre-closure phase.

Figure 17ab refers to the pre-closure phase for Expts. 5 and 11, with experimental profiles sampled in several sections at different times and the continuous curve representing

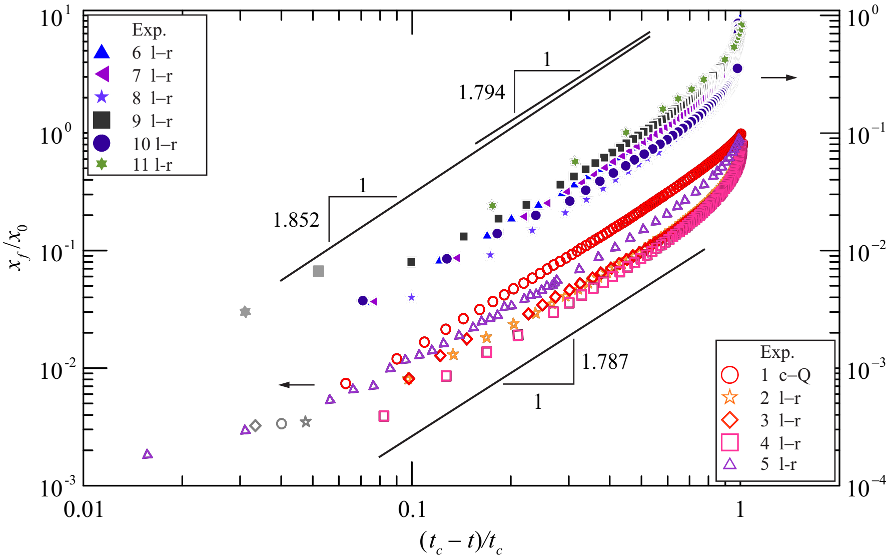

FIGURE 16. Front position of gravity currents in converging channel flow with $k = 0.6$. Experiments 1–5 refer to Newtonian fluid (left vertical axis), experiments 6–11 refer to shear-thinning fluids /right vertical axis). The straight lines correspond to the theoretical curves for $n = 1$ and $n = 0.54-0.90$, respectively, with eigenvalues $\delta_c = 1.787$ and $\delta_c = 1.852-1.794$. The parameters of the experiments are listed in Table 1.

the theoretical model. For the Newtonian fluid case, the early time profiles show a significant discrepancy with theory, which however decreases after approximately 190 s. That means that at least for approximately 35 s the current is in self-similar regime, ended by the insurgence of capillarity effects near the origin. For the power-law fluid, Exp. 11, the profile at $t = 6$ s differs from the rest of the time snapshots which collapse onto one curve, so they are self-similar; all profiles differ from theory at the peak around $\xi/\xi_f \approx 2.5$ and are in excess to the same degree that the profile at $t = 6$ s differs around $\xi/\xi_f \approx 10$, and is in defect. We observe that Exp. 11 has the highest initial Reynolds number and shows an initial stage when inertial effects are comparable to viscous ones. However, the current forgets its original regime and evolves towards self-similarity. This is another validation of the memoryless behaviour of the gravity currents, which not only forget the type of influx (lock-release or constant influx), but also their initial regime (inertial or in transition). The analysis of the time requested by self-similar solutions to approximate within a given accuracy the (numerical) solutions was discussed by Ball *et al.* (2017); Ball & Huppert (2019) in the context of gravity currents, also considering different shapes of the lock or inflow rate variations. The results obtained for first-kind self-similar solutions can be extended to experiments and to second-kind self-similar processes: the approximation improves with time, unless disturbances effects (like capillarity) render the model invalid. It explains the different agreement in times between experiments and theory, which improves for $t > 6$ s although the peak value of H is underestimated by approximately 15%. The numerous approximations of the model are responsible for this discrepancy, but the self-similar nature of the profiles is adequately confirmed.

A comparison between experiments and theory has been conducted also for the post-closure stage, with the current levelling near the origin. In this case the pre-factor refers to the time evolution of the current depth in the origin, where, in the self-similar stage,

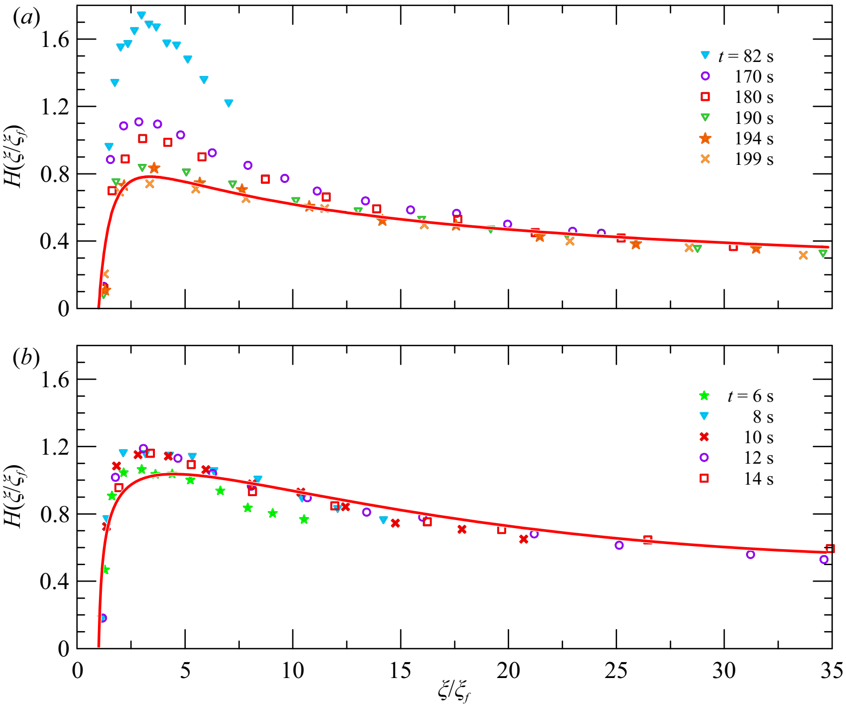

FIGURE 17. Experimental profiles of the current in converging channel flow with $k = 0.6$ during pre-closure (symbols) compared to the theoretical self-similar solution (bold line). (*a*) Exp. 5, Newtonian fluid, $t_c = 229$ s, $\delta_c = 1.7874$, $\alpha = 0.30$; (*b*) Exp. 11, power-law fluid, $t_c = 16.4$ s, $\delta_c = 1.8534$, $\alpha = 0.19$.

results

$$\frac{h(0,t)}{h_\infty} = \alpha' \left(\frac{-t_r}{t_c}\right)^{\delta_c(n+1)(1-k)-n}. \tag{4.7}$$

Figure 18 shows the comparison between theory and experiments for Exp. 5 and 11. During post-closure, the pre-factor α' is computed by considering the experimental time evolution of the depth $h(0,t)$, which is initially varying according to eq.(4.7), see the insets. The theoretical exponent of the current depth growth in the origin is $\delta_c(n+1)(1-k)-n$, equal to 0.429 and to 0.602 for Exp. 5 and Exp. 11, respectively; the experimental values are 0.42 and 0.51, with a fairly good agreement for the first one, an acceptable agreement for the second one. The overall adherence between experiments and theory is striking, with a better collapse of the experimental data and of the theoretical curve for increasing time after closure.

The theoretical formulation for converging radial currents was also experimentally validated. Figure 19 shows the time position of the front of the current in radial geometry: experiments are divided in two groups with Newtonian and shear-thinning fluids, respectively. The Newtonian fluid case was already validated by Diez *et al.* (1992*b*). Exp. 19 and 20 have very different closure times and different time evolution of the front position, although the characteristics of the fluid are practically similar, the only difference being the density, for both fluids a few percent larger than the water, the ambient fluid. As an explanation of this anomaly, we remind that the difference in density is small, but the reduced gravity appearing in buoyancy is significantly different. In addition, both tests are partially influenced by diffusive processes which further reduce the density difference

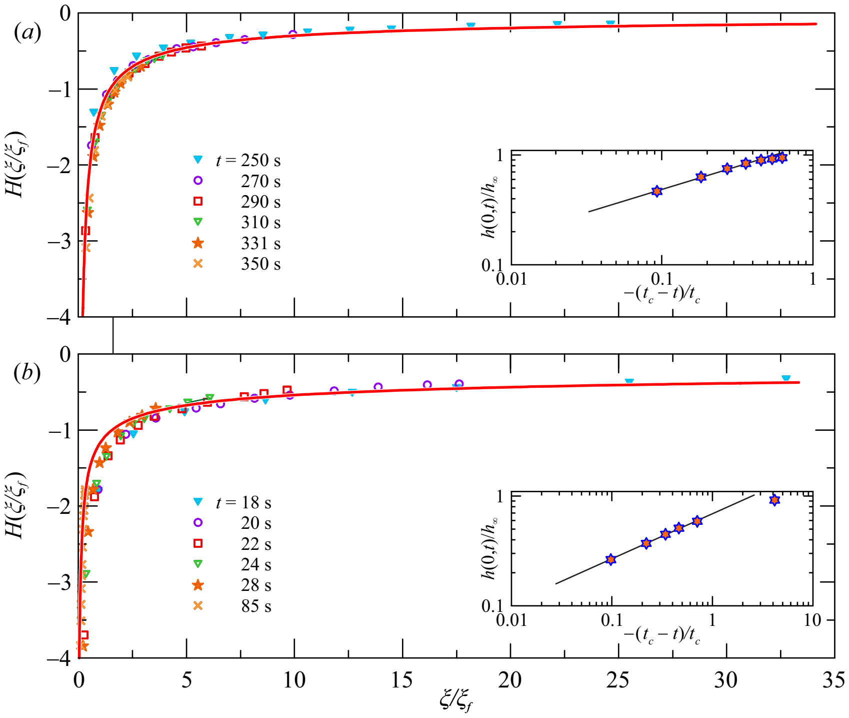

FIGURE 18. Experimental profiles of the current in converging channel flow with $k = 0.6$ during levelling (symbols) compared to the theoretical self-similar solution (bold line). (*a*) Exp. 5, Newtonian fluid $n = 1$, $t_c = 229$ s, $\delta_c = 1.7874$, $\alpha' = 1.29$; (*b*) Exp. 11, power-law fluid $n = 0.54$, $t_c = 16.4$ s, $\delta_c = 1.8534$, $\alpha' = 0.41$. The insets are the time level series at the origin adopted to estimate the pre-factor α'.

between the current and the ambient fluid, to a greater extent for Exp. 19 (less dense current fluid of the two) than for Exp. 20 (denser fluid of the current between the two). Ultimately, under such experimental conditions small variations in the parameters can amplify differences.

In radial geometry the eigenvalue has an almost constant value for $n > 0.8$ although a significant deviation from the average value of ≈ 0.78 can be observed only for very shear-thinning fluids. Observing the time series of the front position, there are no significant differences for experiments in full circle and partial circle configuration, and also the different mode of inflow does not apparently affect the results. However, we expect that the two different geometries, the circular sector and the full-circle, can guarantee the experimental reproduction of self-similarity for different time intervals. In the case of the circular sector, when the current is approaching closure the flow field becomes three-dimensional, with comparable tangential stresses in the vertical planes; moreover, capillarity introduces, for the circular sector, disturbances that are not present in full-circle geometry. In summary, the full-circle provides the conditions for the establishment of self-similarity more than the circular sector. This happens to a greater extent the smaller the angle at the centre of the circular sector.

The agreement between theory and experiments is generally good, with some dispersion of the data when the current is near the closure, due to the dominance of interferences. The early stage adaptation to the self-similar solution has a different duration for different tests, but the duration of the intermediate self-similar regime is always quite long.

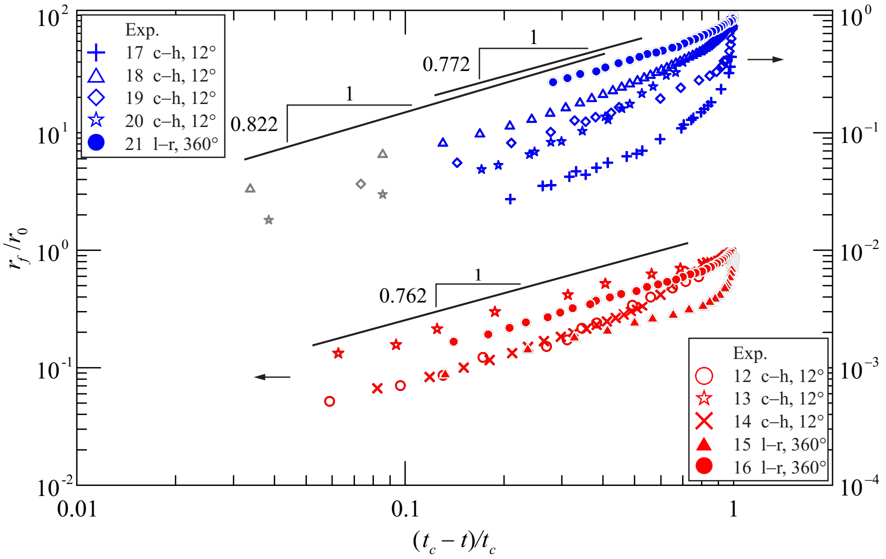

FIGURE 19. Front position of gravity currents in radial converging flow. Experiments 12–16 refer to Newtonian fluid (left vertical axis), experiments 17–21 refer to shear-thinning fluids (right vertical axis). The straight lines correspond to the theoretical curves for $n = 1$ and $n = 0.29-0.63$, respectively, with eigenvalues $\delta_c = 0.762$ and $\delta_c = 0.822-0.772$. The parameters of the experiments are listed in table 1.

5. Conclusion

We conducted an analysis of gravity currents advancing toward the origin in a channel, or fracture, of variable gap thickness and in radial geometry. Previous studies had discovered a second-kind self-similarity solution for Newtonian fluids and provided its experimental validation. Here, we have extended the analysis to power-law fluids, a useful approximation of some real complex fluids frequently adopted in industrial and environmental applications. The theoretical analysis was focussed on the behaviour of the solution about the singular points in the phase plane, computing the limiting eigenvalues consistent with the physical behaviour of the current, and was followed by numerical integration for the pre-closure and post-closure phase, respectively. A quite long converging channel was built to favour the experimental onset of the self-similarity regime, and two other tanks where also constructed, with two different radial geometries, a full radial and a sector 12° wide. The experiments were conducted with dam-break, constant head and constant inflow rate; in all cases the self-similarity was achieved as detected by measuring the front position in time, giving evidence that the initial conditions do not influence the propagation of the current after a certain time lag. The achievement of the self-similar condition is faster for constant inflow rate than for lock release or constant head. This is a major difference with respect to gravity currents propagating with a self-similar regime of the first-kind, which, for example, experimentally do not depend on the precise geometry of the injector (Lyle *et al.* 2005), but till have a different shape depending on whether the overall volume of the current is constant or varies with time. We remind that the behaviour of the second-kind self-similar currents is predicted by the singular points joined by the integral curve. From the experimental point of view this dependence is not so strong, and any case the injection mode influences the time required to reach self-similarity. The existence of an experimental self-similarity confirms that the theoretical solution is also stable.

Specific findings are as follows:

- The eigenvalue for converging channel flow is influenced more by the fracture geometry (width parameter k) than by the fluid nature (flow behaviour index n); it approaches unity for $k \to 0$ and infinity for $k \to 1$ (a wedge-like channel); its minimum value increases with n and k.
- Relative differences between eigenvalues corresponding to different values of n are modest until $k \leqslant 0.7$, then increase rapidly, especially for low n values (very shear-thinning fluids).
- The critical eigenvalue has bounds $n/[(n+1)(1-k)] < \delta_c < 1/(1-k)$, with the upper bound independent of the fluid nature.
- Levelling near the origin implies a time exponent less than unity for the growth of the current depth; levelling is faster for very shear-thinning fluids and lower values of width parameter k.
- In the case of radial converging flow, results for eigenvalues are qualitatively similar to those for channel flow; in particular, the critical eigenvalue has an average value of ≈ 0.78, an almost constant value for $n > 0.8$ and shows a significant increase from the average value only for very shear-thinning fluids (low n).

Perspectives for future extension include the adoption of more realistic rheological models of widespread use in technical applications, such as Herschel-Bulkley (three-parameter) or truncated power-law (four-parameter). For example, a preliminary analysis shows that for a Herschel-Bulkley fluid the present approach brings to a spatial (three dimensional) ODE system, with three dependent variables; this is in variance with the present work on converging motion of power-law fluids in channelized or radial flow, where a planar system of equations arises. Insofar, such problems have not arisen in this sub-field of fluid mechanics.

Other classical effects often included in gravity current modelling, such as fluid infiltration or ex-filtration due e.g. to a porous substrate, need attention: these phenomena imply source/sink terms representing mass addition or subtraction and complicating the differential problem. Similar issues arise with chemical reactions. Also, surface tension effects can be dominant in very thin fractures, almost ubiquitous in many natural formations, and require a proper analysis in order to be included in the model.

As a last point, possible extensions include the analysis of converging currents with non-axisymmetric geometry of the holes, following the analysis performed for Newtonian fluids in Angenent *et al.* (2001); Diez *et al.* (1998).

Acknowledgements

S.L. gratefully acknowledges the financial support from Anton Paar for co-funding Anton Paar DMA 5000 density meter and TwineDrive MCR 702 rheometer. The Department of Engineering and Architecture, with its Rheometrica lab, is in the list of the Anton Paar reference research centres for the testing and development of experimental apparatus in the field of rheology. The cost of the equipment used for this experimental investigation was partly supported by the University of Parma through the Scientific Instrumentation Upgrade Programme 2018. V.D.F. gratefully acknowledges the financial support from Università di Bologna 'Almaidea 2017 Linea Senior grant' and 'Ricerca Fondamentale Orientata (RFO) 2017'.

Declaration of Interests

The authors report no conflict of interest.

	$k = 0.5$	0.6	0.7	0.8	0.9	0.95	0.98
$n = 0.3$	1.6505436	1.9860302	2.5629732	3.77226735	7.595576765	15.30827880	38.39318184
0.5	1.5836860	1.8674737	2.3408605	3.30194250	6.333355500	12.87070894	33.03107487
0.7	1.5555845	1.8153570	2.2396420	3.07693480	5.590929700	10.74155645	27.17726191
1.0	1.5422697	1.7874093	2.1826545	2.95561600	5.279916050	10.08649685	25.03621420
1.5	1.5479785	1.7901284	2.1841454	3.01639213	6.000000576	12.00000031	30.0

TABLE A.1. Eigenvalues evaluated for converging flow in a channel of gap thickness $b = b_1 x^k$ for different values of k and of fluid behaviour index n.

n	δ_c	n	δ_c	n	δ_c
0.1	0.880292	0.6	0.775568	1.1	0.760562
0.2	0.833010	0.7	0.770503	1.2	0.759517
0.3	0.808010	0.8	0.766795	1.3	0.758815
0.4	0.792737	0.9	0.764035	1.4	0.758394
0.5	0.782610	1.0	0.762035	1.5	0.758206

TABLE A.2. Eigenvalues evaluated for converging radial gravity flow for different fluid behaviour index n.

Appendices

A. Numerical values of δ_c

Table A.1 and table A.2 list the eigenvalues computed for converging gravity flow of a power-law fluid in a channel of varying gap thickness and in radial geometry, respectively.

B. Flow in a porous medium of varying permeability and porosity and Hele-Shaw analogy

Consider a plane gravity current of a power-law fluid propagating on a horizontal impermeable bottom toward the origin of a porous domain saturated by a lighter fluid at rest; motion is driven by the density difference $\Delta\rho$ between the two fluids. The current is released at a distance x_0 from the origin and reaches it at time t_c. Under the assumptions of (i) sharp interface, (ii) thin intruding current, (iii) negligible capillarity effects, the spreading is described by the current height $h(x,t)$, vertical velocities are neglected, and pressure is hydrostatic with $\partial p/\partial x = \Delta\rho\, g(\partial h/\partial x)$. The porous domain is heterogeneous with deterministic variations in permeability k and porosity ϕ along the horizontal direction x given by

$$\phi(x) = \phi_1 x^{\gamma}, \quad k(x) = k_1 x^{\beta}, \tag{B.1}$$

where ϕ_1, k_1 are costants of dimensions $[L^{-\gamma}]$ and $[L^{2-\beta}]$ respectively, and γ, β are dimensionless non-negative constants; for a homogeneous medium $\gamma = \beta = 0$.

The filtration law for the power-law fluid described by eq.(2.1) is given by (Di Federico *et al.* 2014)

$$\nabla p - \rho \mathbf{g} = -\frac{1}{\Lambda k^{(n+1)/2}} \left|\mathbf{v}\right|^{n-1} \mathbf{v}; \Lambda = \Lambda(\phi, \mu_0, n) = \frac{8^{(n+1)/2}}{2} \left(\frac{n}{3n+1}\right)^{n} \frac{\phi^{(n-1)/2}}{\mu_0} \tag{B.2}$$

with p pressure, $\mathbf{g}$ gravity, $\mathbf{v} \equiv (u, v, w)$ Darcy velocity. The mass balance for 1-D flow reads

$$\frac{\partial}{\partial x}\left(\int_0^h u\,dz\right) = -\frac{\partial}{\partial t}\left(\int_0^h \phi\,dz\right). \tag{B.3}$$

Substituting the horizontal velocity from (B.2) into (B.3) and using (B.1) yields

$$\frac{u_1}{x^\gamma}\frac{\partial}{\partial x}\left[h x^{F_1}\frac{\partial h}{\partial x}\left|\frac{\partial h}{\partial x}\right|^{1/n-1}\right] = \frac{\partial h}{\partial t}, \tag{B.4}$$

with

$$u_1 = \frac{(\Delta\rho\, g/\mu_0)^{1/n}\, k_1^{(n+1)/(2n)}}{\phi_1^{(n+1)/(2n)}}; \quad F_1 = \frac{\gamma(n-1)+\beta(n+1)}{2n}. \tag{B.5}$$

The problem thus stated is amenable to a self-similar solution of the second-kind analogous to that described in section 2 for converging flow in a channel of variable gap thickness. The dimensional counterpart of (B.4) for channel flow is easily derived from eqs.(2.2–2.3) as

$$\frac{u_0}{x^k}\frac{\partial}{\partial x}\left[x^{k(2n+1)/n} h\frac{\partial h}{\partial x}\left|\frac{\partial h}{\partial x}\right|^{1/n-1}\right] = \frac{\partial h}{\partial t}, \tag{B.6}$$

where

$$u_0 = \left(\frac{\Delta\rho g}{\mu_0}\right)^{1/n}\frac{n}{2n+1}\left(\frac{b_1}{2}\right)^{(n+1)/n}. \tag{B.7}$$

Comparing exponents in eq.(B.4) and eq.(B.6) it is seen that the Hele-Shaw analogy for power-law fluids (Ciriello *et al.* 2016) requires

$$\begin{cases}\gamma = k\\ \beta = 3k.\end{cases} \tag{B.8}$$

Under the validity of equations (B.8) the analogy is established and one can proceed as in Section 2, the critical eigenvalues will be the same. The above conditions are however quite restrictive; a wider choice of parameter combinations is available using a mapping parameter, see Appendix A.2 in Ciriello *et al.* (2016).

Non-standard Hele-Shaw cells with tapered plates have been widely applied in thin film flows and slow viscous flows with a moving boundary, see, e.g., Al-Housseiny *et al.* (2012); Dias & Miranda (2013); Al-Housseiny & Stone (2013); Bongrand & Tsai (2018). See also Morrow *et al.* (2019) where non-standard Hele-Shaw cell configuration (tapered of rotating) is investigated aiming to improve the efficiency in controlling interfacial instabilities.

REFERENCES

Al-Housseiny, T. T. & Stone, H. A. 2013 Controlling viscous fingering in tapered hele-shaw cells. *Physics of Fluids* **25** (9), 092102.

Al-Housseiny, T. T., Tsai, P. A. & Stone, H. A. 2012 Control of interfacial instabilities using flow geometry. *Nature Physics* **8** (10), 747–750.

Angenent, S. B. & Aronson, D. G. 1995*a* The focusing problem for the radially symmetric porous medium equation. *Communications in Partial Differential Equations* **20** (7-8), 1217–1240.

Angenent, S. B. & Aronson, D. G. 1995*b* Intermediate asymptotics for convergent viscous gravity currents. *Physics of Fluids* **7** (1), 223–225.

Angenent, S. B., Aronson, D. G., Betelu, S. I. & Lowengrub, J. S. 2001 Focusing of an elongated hole in porous medium flow. *Physica D: Nonlinear Phenomena* **151** (2), 228–252.

Aronson, D. G. & Graveleau, J. 1993 A selfsimilar solution to the focusing problem for the porous medium equation. *European Journal of Applied Mathematics* **4** (1), 65–81.

Aronson, D. G., Van Den Berg, J. B. & Hulshof, J. 2003 Parametric dependence of exponents and eigenvalues in focusing porous media flows. *European Journal of Applied Mathematics* **14** (4), 485.

Aronsson, G. & Janfalk, U. 1992 On Hele–Shaw flow of power-law fluids. *European Journal of Applied Mathematics* **3** (4), 343–366.

Ball, T. V. & Huppert, H. E. 2019 Similarity solutions and viscous gravity current adjustment times. *Journal of Fluid Mechanics* **874**, 285–298.

Ball, T. V., Huppert, H. E., Lister, J. & Neufeld, J. 2017 The relaxation time for viscous and porous gravity currents following a change in flux. *Journal of Fluid Mechanics* **821**, 330–342.

Barenblatt, G. I. 1996 *Scaling, self-similarity, and intermediate asymptotics*. Cambridge University Press.

Barenblatt, G. I. 2003 *Scaling*, , vol. 14. Cambridge University Press.

Barenblatt, G. I. & Zel'Dovich, Y. B. 1972 Self-similar solutions as intermediate asymptotics. *Annual Review of Fluid Mechanics* **4** (1), 285–312.

Bongrand, G. & Tsai, P. A. 2018 Manipulation of viscous fingering in a radially tapered cell geometry. *Physical Review E* **97** (6), 061101.

Carpenter, H. J., Gholipour, A., Ghayesh, M. H., Zander, A. C. & Psaltis, P. J. 2020 A review on the biomechanics of coronary arteries. *International Journal of Engineering Science* **147**, 103201.

Ciriello, V., Longo, S., Chiapponi, L. & Di Federico, V. 2016 Porous gravity currents: a survey to determine the joint influence of fluid rheology and variations of medium properties. *Advances in Water Resources* **92**, 105 – 115.

Ciriello, V., Longo, S. & Di Federico, V. 2013 On shear thinning fluid flow induced by continuous mass injection in porous media with variable conductivity. *Mechanics Research Communications* **52**, 101–107.

Cole, J. D. & Wagner, B. A. 1996 On self-similar solutions of Barenblatt's nonlinear filtration equation. *European Journal of Applied Mathematics* **7** (2), 151–167.

Coussot, P. & Meunier, M. 1996 Recognition, classification and mechanical description of debris flows. *Earth-Science Reviews* **40** (3), 209–227.

Daly, E. & Porporato, A. 2004 Similarity solutions of nonlinear diffusion problems related to mathematical hydraulics and the fokker-planck equation. *PRE* **70** (5), 056303.

Di Federico, V. 1998 Non-Newtonian flow in a variable aperture fracture. *Transport in Porous Media* **30** (1), 75–86.

Di Federico, V., Archetti, R. & Longo, S. 2012 Similarity solutions for spreading of a two-dimensional non-Newtonian gravity current. *Journal of Non-Newtonian Fluid Mechanics* **177–178**, 46–53.

Di Federico, V., Longo, S., Chiapponi, L., Archetti, R. & Ciriello, V. 2014 Radial gravity currents in vertically graded porous media: theory and experiments for Newtonian and power-law fluids. *Advances in Water Resources* **70**, 65–76.

Dias, E. O. & Miranda, J. A. 2013 Taper-induced control of viscous fingering in variable-gap Hele-Shaw flows. *Physical Review E* **87** (5), 053015.

Didden, N. & Maxworthy, T. 1982 The viscous spreading of plane and axisymmetric gravity currents. *Journal of Fluid Mechanics* **121**, 27–42.

Diez, J. A., Gratton, J. & Minotti, F. 1992*a* Self-similar solutions of the second kind of nonlinear diffusion-type equations. *Quarterly of Applied Mathematics* **50** (3), 401–414.

Diez, J. A., Gratton, R. & Gratton, J. 1992*b* Self-similar solution of the second kind for a convergent viscous gravity current. *Physics of Fluids A: Fluid Dynamics* **4** (6), 1148–1155.

Diez, J. A., Thomas, L. P., Betelú, S., Gratton, R., Marino, B., Gratton, J., Aronson,

D. G. & Angenent, S. B. 1998 Noncircular converging flows in viscous gravity currents. *Physical Review E* **58** (5), 6182.

Eggers, J. & Fontelos, M. A. 2015 *Singularities: formation, structure, and propagation*, , vol. 53. Cambridge University Press.

Epelle, E. I. & Gerogiorgis, D. I. 2020 A review of technological advances and open challenges for oil and gas drilling systems engineering. *AiChe Journal* **66** (4).

Eshtiaghi, N., Markis, F., Yap, S. D., Baudez, J.-C. & Slatter, P. 2013 Rheological characterisation of municipal sludge: A review. *Water Research* **47** (15), 5493–5510.

Ghodgaonkar, A. A. 2019 Numerical methods for studying self-similar propagation ov viscous gravity currents. Master's thesis, Purdue University, West Lafayette, Indiana.

Gratton, J. & Minotti, F. 1990 Self-similar viscous gravity currents: phase-plane formalism. *Journal of Fluid Mechanics* **210**, 155–182.

Gratton, J., Minotti, F. & Mahajan, S. M. 1999 Theory of creeping gravity currents of a non-Newtonian liquid. *Physical Review E* **60(6)**, 6960–6967.

Gratton, J. & Perazzo, C. A. 2010 Self-similar collapse of a circular cavity of a power-law liquid. *Journal of non-Newtonian Fluid Mechanics* **165** (3-4), 158–162.

Huppert, H. E. 1982 The propagation of two-dimensional and axisymmetric viscous gravity currents over a rigid horizontal surface. *Journal of Fluid Mechanics* **121**, 43–58.

Huppert, H. E. 2006 Gravity currents: a personal perspective. *Journal of Fluid Mechanics* **554**, 299.

Huppert, H. E. & Woods, A. W. 1995 Gravity-driven flows in porous layers. *Journal of Fluid Mechanics* **292**, 55–69.

Kondic, L., Palffy-Muhoray, P. & Shelley, M. J. 1996 Models of non-Newtonian Hele-Shaw flow. *Physical Review E* **54** (5), R4536.

Kondic, L., Shelley, M. J. & Palffy-Muhoray, P. 1998 Non-Newtonian Hele-Shaw flow and the Saffman-Taylor instability. *Physical Review Letters* **80** (7), 1433.

Lareo, C., Fryer, P. J. & Barigou, M. 1997 The fluid mechanics of two-phase solid-liquid food flows: A review. *Food and Bioproducts Processing* **75** (C2), 73–105.

Lauriola, I., Felisa, G., Petrolo, D., Di Federico, V. & Longo, S. 2018 Porous gravity currents: Axisymmetric propagation in horizontally graded medium and a review of similarity solutions. *Advances in Water Resources* **115**, 136–150.

Livescu, S. 2012 Mathematical modeling of thixotropic drilling mud and crude oil flow in wells and pipelines - a review. *Journal of Petroleum Science and Engineering* **98 - 99**, 174 – 184.

Longo, S., Ciriello, V., Chiapponi, L. & Di Federico, V. 2015*a* Combined effect of rheology and confining boundaries on spreading of porous gravity currents. *Advances in Water Resources* **79**, 140–152.

Longo, S. & Di Federico, V. 2015 Unsteady flow of shear-thinning fluids in porous media with pressure-dependent properties. *Transport in Porous Media* **110** (3), 429–447.

Longo, S., Di Federico, V. & Chiapponi, L. 2015*b* Non-Newtonian power-law gravity currents propagating in confining boundaries. *Environmental Fluid Mechanics* **15** (3), 515–535.

Lyle, S., Huppert, H. E., Hallworth, M., Bickle, M. & Chadwick, A. 2005 Axisymmetric gravity currents in a porous medium. *Journal of Fluid Mechanics* **543**, 293–302.

McCue, S. W., Jin, W., Moroney, T. J., Lo, K.-Y., Chou, S.-E. & Simpson, M. J. 2019 Hole-closing model reveals exponents for nonlinear degenerate diffusivity functions in cell biology. *Physica D: Nonlinear Phenomena* **398**, 130–140.

McCue, S. W. & King, J. R. 2011 Contracting bubbles in hele-shaw cells with a power-law fluid. *Nonlinearity* **24** (2), 613.

Morrell, R. S. & De Waele, A. 1920 *Rubber, resins, paints and varnishes*. Nostrand.

Morrow, L. C., Moroney, T. J. & McCue, S. W. 2019 Numerical investigation of controlling interfacial instabilities in non-standard Hele-Shaw configurations. *arXiv preprint arXiv:1901.00288* .

Ostwald, W. 1929 Ueber die rechnerische darstellung des strukturgebietes der viskosität. *Colloid & Polymer Science* **47** (2), 176–187.

Perazzo, C. A. & Gratton, J. 2003 Thin film of non-Newtonian fluid on an incline. *Physical Review E* **67** (1), 016307.

Perazzo, C. A. & Gratton, J. 2005 Exact solutions for two-dimensional steady flows of a power-law liquid on an incline. *Physics of Fluids* **17(1)**, 013102.

Simpson, J. E. 1982 Gravity currents in the laboratory, atmosphere, and ocean. *Annual Review of Fluid Mechanics* **14**, 213–234.

Slim, A. C. & Huppert, H. E. 2004 Self-similar solutions of the axisymmetric shallow-water equations governing converging inviscid gravity currents. *Journal of Fluid Mechanics* **506**, 331.

Stokes, G. G. 1880 On the theory of oscillatory waves. *Transactions of the Cambridge Philosophical Society* .

Wagner, B. 2005 An asymptotic approach to second-kind similarity solutions of the modified porous-medium equation. *Journal of Engineering Mathematics* **53** (3-4), 201–220.

Wolfram Research, Inc. 2017 Mathematica, Version 11.1. Champaign, IL, 2017.

Zheng, Z., Christov, I. C. & Stone, H. A. 2014 Influence of heterogeneity on second-kind self-similar solutions for viscous gravity currents. *Journal of Fluid Mechanics* **747**, 218–246.

Zheng, Z., Shin, S. & Stone, H. A. 2015 Converging gravity currents over a permeable substrate. *Journal of Fluid Mechanics* **778**, 669–690.